Electrical Power and Energy Systems 129 (2021) 106761

Contents lists available at ScienceDirect

International Journal of Electrical Power and Energy Systems

journal homepage: www.elsevier.com/locate/ijepes

MILP model for volt-var optimization considering chronological operation of distribution systems containing DERs

Bibiana P. Ferraz *, Mariana Resener, Luís A. Pereira, Flávio A.B. Lemos, Sérgio Haffner

Universidade Federal do Rio Grande do Sul, Porto Alegre, RS, Brazil

ARTICLE INFO

Keywords:
Operation planning of distribution system
Volt-var control
Mixed-integer linear programming
K-means clustering
Chronological operation

ABSTRACT

This paper presents a mixed-integer linear programming model for volt-var optimization considering the chronological operation of distribution systems containing distributed energy resources (DERs). The proposed model describes the operation problem of capacitor banks (CBs) and voltage regulators (VRs), and it is further based on the steady-state operation during each time interval contained in typical scenarios of distribution systems. A procedure using a K-means clustering algorithm is used to select the scenarios, thus preserving the simultaneity and chronological combination of different loads and DERs. According to the formulation that we developed, the regulation devices become sensitive to downstream load variations, since we use explicit current variables to control automatic CBs, and since we include means to compensate voltage drops along distribution lines in the control of VRs. The model is validated by comparing the results obtained during several tests of two typical cases with those obtained through nonlinear power flow. The typical case studies presented in the paper highlight the good agreement between the results obtained with the linearized model and with power flow method; further, the practical results confirm that the use of typical scenarios allows representing different levels of loads and DERs, while keeping the validity and performance of the proposed model.

1. Introduction

The main goals of the operation planning of power distribution systems (PDS) are to improve efficiency and reduce operation costs [1]. Both goals require an adequate level of node voltages throughout the entire system, which can be achieved by utilizing several strategies and devices. One commonly employed strategy is the volt-var optimization (VVO), used to regulate the voltage magnitude within permissible limits and simultaneously minimize energy losses. Further, efficient and low-cost operation of PDS also requires reactive power control. In this context, reactive power and voltage control in PDS are typically achieved by using coordination schemes comprising several devices, such as shunt fixed and automatic capacitor banks (CBs), voltage regulators (VRs), on-load tap changers (OLTC), and distributed energy resources (DERs). Besides, volt-var control (VVC) devices can also be used, since they are recognized as an effective solution to both reduce energy losses and keep the system operating under given constraints [2].

Several models for VVO have been proposed in recent years. However, due to the discrete nature of the OLTC and capacitor bank switching, as well as the nonlinear power flow constraints, the majority of known models consist of a problem of mixed-integer nonlinear programming (MINLP) [3]. To handle this type of problem, the solution space is simplified using heuristics. For example, through an algorithm based on the hunting mechanism of the gray wolf in nature, the authors of [4] solved the MILNP problem of coordinating the operation of VVC and network reconfiguration to minimize the energy demand. In addition, the presence of DERs was also considered by optimizing the operation of the static inverters controlling the photovoltaic sources so that more energy can be saved. The gray wolf optimization was also used by [5] to minimize voltage deviations with VRs and CBs. A multi-objective optimization problem was proposed in [6] to define strategies for active distribution networks based on VVC, where the authors solved the problem by using Pareto front of non-dominated sorting genetic algorithm (NSGA-II). It is worthwhile noting that although meta-heuristics became increasingly popular because they employ derivative-free techniques, these algorithms do not guarantee optimal solutions.

An interesting way to obtain optimal solutions to nonlinear problems is the use of piecewise linearization (PWL), which leads to a mixed-integer linear programming (MILP) problem [7]. PWL has also been successfully applied to the solution of nonlinear problems with integer

* Corresponding author.
E-mail address: bibiana.petry@ufrgs.br (B.P. Ferraz).

https://doi.org/10.1016/j.ijepes.2021.106761
Received 30 April 2020; Received in revised form 1 October 2020; Accepted 27 December 2020
Available online 2 March 2021

Nomenclature

Sets

ψ^B network branches
ψ^{CB} nodes with capacitor bank
ψ^D loaded nodes
ψ^G nodes with distributed energy resources
ψ^J time intervals of a scenario
ψ^K scenarios
ψ^{VR} nodes with voltage regulator

Integer and binary variables

$r_{i,m,j,sc}$, $rr_{m,j,sc}$ auxiliary binary variables used to obtain the tap position at time interval j of scenario sc of the voltage regulator installed at node m; where $i = 1, 2, \ldots, 6$
$t^{\mathrm{VR}}_{m,j,sc}$ integer variable representing the tap position at time interval j of scenario sc of the voltage regulator installed at node m (variable position of under-load tap changer)
$w^{AI}_{m,j,sc}$ binary variable related to the switch operation of an automatic capacitor bank of type I installed at node m; when $w^{AI}_{m,j,sc} = 1$, the capacitor switches on or off at time interval j of scenario sc
$y^{AI}_{m,j,sc}$ binary variable related to the operation of an automatic capacitor bank of type I installed at node m; when $y^{AI}_{m,j,sc} = 1$, the capacitor is under operation at time interval j of scenario sc
$w^{\mathrm{VR}}_{m,j,sc}$ binary variable related to the tap operation of an voltage regulator installed at node m; when $w^{AI}_{m,j,sc} = 1$, the regulator is turned on or off at time interval j of scenario sc

Continuous variables and their limits

$\Delta\mathbf{f}^{\mathrm{Re}}_{j,sc}$, $\Delta\mathbf{f}^{\mathrm{Im}}_{j,sc}$ vectors of change in current flow upstream of voltage regulators at time interval j of scenario sc [pu]
$\Delta f^{\mathrm{Re}}_{m,j,sc}$, $\Delta f^{\mathrm{Im}}_{m,j,sc}$ change in current flow at time interval j of scenario sc, upstream of the voltage regulator installed at node m [pu]
ΔT_{sc} scenario duration sc [days]
$\Delta V_{m,j,sc}$ change in voltage at time interval j of scenario sc due to a voltage regulator installed at node m [pu]
$\mathbf{d}^{\mathrm{Re}}_{j,sc}$, $\mathbf{d}^{\mathrm{Im}}_{j,sc}$ vectors of real and imaginary load currents at time interval j of scenario sc [pu]
$\mathbf{f}^{\mathrm{Re}}_{j,sc}$, $\mathbf{f}^{\mathrm{Im}}_{j,sc}$ vectors of real and imaginary branch currents at time interval j of scenario sc [pu]
$\mathbf{g}^{\mathrm{Re}}_{j,sc}$, $\mathbf{g}^{\mathrm{Im}}_{j,sc}$ vectors of real and imaginary current injections at time interval j of scenario sc [pu]
$\mathbf{P}^{D}_{j,sc}$, $\mathbf{Q}^{D}_{j,sc}$ matrices of active and reactive power demands of loads at time interval j of scenario sc [pu]
$\mathbf{q}^{A}_{j,sc}$ vector of automatic capacitor banks current injections at time interval j of scenario sc [pu]
$\mathbf{V}_{j,sc}$ vector of voltage magnitudes at time interval j of scenario sc [pu]
$a_{m,j,sc}$ transformation ratio of voltage regulator at node m at time interval j of scenario sc
$d^{\mathrm{Re}}_{m,j,sc}$, $d^{\mathrm{Im}}_{m,j,sc}$ real and imaginary parts of load current at node m at time interval j of scenario sc [pu]
$f^{\mathrm{Re}}_{km,j,sc}$, $f^{\mathrm{Im}}_{km,j,sc}$ real and imaginary parts of the current in branch km at time interval j of scenario sc [pu]
$g^{\mathrm{Re}}_{m,j,sc}$, $g^{\mathrm{Im}}_{m,j,sc}$ real and imaginary parts of the current injection at node m during time interval j of scenario sc [pu]
$I^{\mathrm{trs},AI}_{m,j,sc}$ transition current at time interval j of scenario sc, used in automatic capacitor bank control installed at node m [pu]
$I^{\mathrm{on},AI}_{m}$, $I^{\mathrm{off},AI}_{m}$ currents to switch on and off the automatic capacitor bank of type I installed at node m [pu]
$K_{km,j,sc}$ adjustment factor to calculate the voltage drops in the branch km at time interval j of scenario sc
P^D, Q^D active and reactive power demands of loads [pu]
P^G active power injection of distributed energy resources [pu]
$p^{\mathrm{loss}}_{km,j,sc}$ power losses of branch km at time interval j of scenario sc [pu]
$V_{m,j,sc}$ voltage magnitude at node m at time interval j of scenario sc [pu]
$V^{\mathrm{set,VR}}_{m}$ set voltage to be held by a voltage regulator installed at node m [pu]
$z_{m,j,sc}$ voltage violation at node m during time interval j of scenario sc [pu]
ΔT_{sc} time interval duration sc [hour]

Parameters

β voltage regulator bandwidth [pu]
ΔI bandwidth of capacitor bank control [pu]
$\mathbf{S}$ node-branch incidence matrix of the system
C^{kWh} energy cost [US$/kWh]
C^{oper} total operation costs [US$]
C^{loss}_{sc} cost of energy losses for scenario sc [US$]
C^{vio}_{sc} cost of voltage violations for scenario sc [US$]
CV linear penalty factor for violation of voltage limits [US $/time interval]
M big number used in the inequalities of disjuntive constraints
R_{km}, X_{km} real and imaginary part of the impedance of the branch km [pu]
S_{base} base power [kVA]
$W^{\mathrm{max},AI}_{m,sc}$ limit of daily switching of automatic capacitor banks
$W^{\mathrm{max,VR}}_{m,sc}$ limit of tap operation of voltage regulators

variables, since PWL can be used to obtain optimal solutions through exact optimization methods with guaranteed convergence. As an example, a linearized model was proposed by the authors of [8] to determine the steady-state operation of PDS without using nonlinear power flow. The problem of CB allocation was solved by analyzing operational costs, including voltage violations and power losses, which were estimated using PWL. Further, the optimal allocation of VRs, the problem of reconductoring, and the operation of DERs were included in the MILP formulation proposed in [9,10]. A relevant advantage of the representation of voltage limits proposed by [9] is the use of auxiliary variables and linear constraints, thus avoiding strict limits on the voltage magnitude at the nodes, so that the problem rarely becomes infeasible. Additionally, an alternative approach to nonlinear model was proposed by [11], where a mixed-integer, quadratically constrained programming problem was solved by modeling the voltage-dependent elements aiming at improving the accuracy of VVO.

Regarding known VVO approaches, the optimal operation problem of PDS was addressed in [12] through mixed-integer second-order cone programming and MILP models. The control variables considered were the active and reactive power of dispatchable distributed generation, the number of switchable CB units in operation, the tap position of VRs, and the operation state of energy storage devices. According to the model described in [12], the switching mechanism of VRs is remotely controlled; on the other hand, the authors show results concerning 72

hours. In [13], a framework considering VVC was proposed for the problem of coordination of electric vehicle (EV) charging in distribution systems. In this framework, a MILP model was solved to minimize the costs of the energy purchased from the substation and distributed generation; energy curtailment of EVs and storage units; and energy injected from storage units. The framework also includes VVC strategies to define the taps of VRs, as well as strategies to switch on CB units for 24 hours. A MILP model for the VVC problem in unbalanced distribution systems was proposed by [14], aiming to minimize voltage and power factor violations and the active power consumption from the substation. This model handled the VVC by coordinating the operation of transformers with OLTC, distributed generators, and switchable CBs.

The major common drawback of the models presented in [9,12–14] is that the VVC devices are remotely controlled based on a centralized approach, which often does not correspond to the way distribution systems operate. Besides, decentralized approaches are more difficult to implement in practice, since they require efficient local VVC schemes which at the same time help find out the optimal solution of the entire distribution system. Additionally, local adjustments of the VVC devices are in part dictated by the accuracy of the load description and the behavior of DERs models. Besides, deterministic approaches, for which worst-case scenarios are assumed, disregard the uncertainties arising from the stochastic nature of both loads and DERs. Thus, a transition from deterministic to probabilistic power flow analysis is required [15].

Since nowadays PDS contain many DERs and given their inherent stochastic behavior, researchers and planners are spending great efforts in developing approaches for VVO for PDS involving uncertainty. Thus, a novel stochastic programming model for active and reactive power scheduling was proposed by [16] to manage the daily VVC. Based on selected random scenarios of renewable power generation, the stochastic problem was decomposed into several deterministic problems, each with a different probability. To achieve the VVO, [16] used a generic reactive power bidding structure, modeled through the capability curve of a distributed generation proposed by [17]. In [18], a method to jointly schedule active and reactive power based on costs was proposed to coordinate distributed generation, OLTCs, and switched CBs in smart distribution systems. Additionally, in [19] the author researched the contribution of DERs to VVO, as well as the cost of reactive power, and the inclusion of demand response. Further, the authors of [20] proposed an active-reactive power model based on bids which aims to deal with the scheduling of energy/reactive power resources in PDS with the integration of many DERs. A common characteristic of all the cited studies [16–20] is that they propose mixed-integer nonlinear optimization problems. Given that such problems can become non-convex having many local minima and a difficult global optimal solution, [21] proposed an algorithm based on Benders decomposition to solve the daily VVC of PDS; this algorithm includes a capability diagram of DERs and considers environmental as well as economic aspects.

Stochastic models can become computationally intensive and highly constrained. In the case of non-convex optimization, multiple locally-optimal solutions are feasible and the use of a larger number of scenarios to describe the uncertainties can increase the accuracy of the solutions [22]. However, using several scenarios can lead to redundancy and a higher computational burden. Therefore, in practice, VVO problems should be solved including only a reduced number of typical periods. As an example, the authors of [23] introduced a novel clustering method which incorporates a K-means clustering algorithm into the MILP model; the method aims to select typical and extreme days which are subsequently used to optimize the design of multi-energy systems.

Due to the practical and technical advantages of clustering techniques in problems related to the design and operation of PDS, these techniques have been extensively applied using many different approaches. A great number of them are discussed in [22,24]. The K-means clustering is one of the most popular and simple clustering algorithms; it was used by [4,22,25–27] to group year profiles of loads and DERs within PDS, thus reducing the number of system states. As an important advantage, the clusters thus defined preserved the correlation between quantities of different nature, e.g. loads and DERs; besides, these clusters are also used to solve the operational slave problem of multi-level optimization models [25–27].

1.1. Main contributions

Although VVO models have already been investigated, to our knowledge, no previous work proposed a MILP with explicit control variables to determine the optimal adjustment of CBs and VRs. We formulate the current control of automatic CBs using piecewise linear functions; we also model the VR control with line drop compensator (LDC) to optimally regulate remote node voltages; further, the VR control is designed to take into account the possibility of saturation under specific operating conditions. However, the major advantage of the method we propose is the definition and use of a MILP model for VVO of CBs and VRs that considers the chronological operation and the inherent simultaneity of multiple loads and DERs. In addition, we use electrical quantities to formulate volt-var control, thus making our model better than similar models and suitable for practical applications in decentralized VVC schemes.

In the context thus far described, this paper contributes to existing studies in the following aspects:

i. we introduce a linearized model to determine the steady-state operation during each time interval within typical daily scenarios of distribution systems with VVC devices and DERs;
ii. we present a scenario approach to preserve simultaneity and chronological combination of different loads and DERs, including both real and reactive power demands;
iii. we formulate a MILP model for VVO that includes the following under the constraints used to restrict the daily switching of VVC devices: (a) explicit current control variables that switch on and off automatic CBs, and (b) explicit adjustments of VRs, including the possibility of using line drop compensators;
iv. we propose a decentralized approach in which the devices are locally controlled so as to obtain the optimal solution for the VVO problem of the whole system.

To validate the model, the results obtained using the MILP model are compared with the solution of the nonlinear load flow. Moreover, numerical results of two typical systems illustrate some of the potential applications of the proposed model.

2. Chronological operation of PDS

The assumption of a unique behavior for unequal loads at different nodes, through typical load duration curves, has been in the practice adopted by many utilities. This assumption implies a complete dependency between loads and can also lead to an overestimation of the current in distribution lines. On the other hand, assuming that all node loads are independent can lead to an underestimation of the currents [28]. Besides, the large penetration of DERs in PDS imposes new challenges to continuously maintain the balance between the generated power and consumer demand. In such circumstances, the evaluation of all possible states of a power system can become an impossible task, due to the large number of possible states [29].

To reduce the complexity of the problems cited in the preceding paragraph, several authors recommend a scenario approach [4,22,25–27], which allows finding representative operation profiles. According to this approach, a reduced number of typical scenarios is extracted from annual prediction profiles, which are further assumed to accurately represent both the time-variable nature and the inherent simultaneity between multiple DERs and load demand [26].

Among the methods found in the literature, K-means clustering has been widely used to process large data-sets due to its acceptable

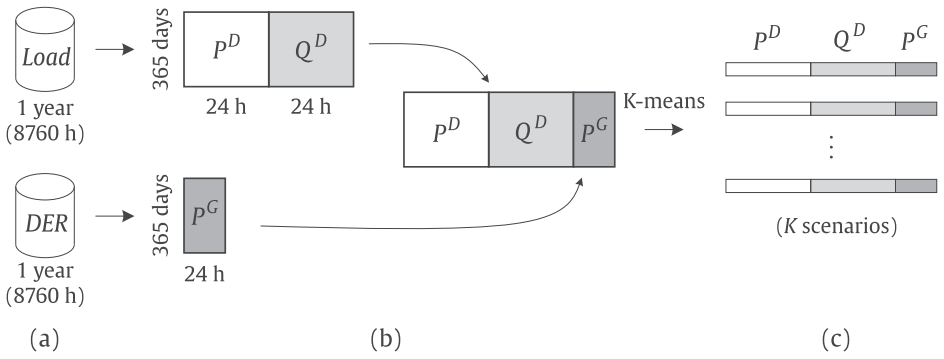

Fig. 1. Definition of scenarios and clusters for chronological operation: (a) raw data; (b) processing of data; (c) selected clusters.

computational efficiency and simple implementation. As thoroughly explained in [24], according to this method, the Euclidean distance is used to evaluate the fitness between points and cluster centers. Further, the number of centroids is determined according to the similarities and proximity of the data points in a way that the correlation between different quantities (e.g. load demand and DERs) is guaranteed. In this way, the historical data are represented by a reduced and tractable number of centroids which depends on the data characteristics and requirements posed by the decision-maker [30].

In an effort to capture an interval-based combination of all loads and DERs, we propose an extension to the scenario approach proposed by [31], as described in what follows. Without loss of generality, the description of the proposed methodology will be made considering a time interval of one hour and a time horizon of one year.

Firstly, as depicted in Fig. 1 (a), data are collected which contains a full-year operation (365 days) of 24-hours profiles of m nodes with loads ($\forall m \in \psi^D$) and DERs ($\forall m \in \psi^G$). Secondly, to represent the annual time-dependent behavior of all loads and DERs, a matrix is created containing the 365 days of the 24-hours behavior of active and reactive power of each load, and also the active power of each DER (see Fig. 1 (b)). Finally, the typical scenarios with similar characteristics are clustered through the K-means algorithm. As a result, the simultaneity and chronological combination of different loads and DERs is preserved through a set of K scenarios, represented by cluster centroids (detailed in Fig. 1 (c)). Thus, the probability of occurrence of each cluster is calculated considering the number of days that the cluster aggregates.

Usually, the balance between computational efficiency and accuracy defines the number of clusters [31]. For this reason, different numbers of clusters are tested and the best number is then chosen based on predefined criteria. In this respect, we propose the use of the *elbow criteria* [32], a common graphical method to evaluate the error of a group of several clusters. The largest error decrease represents the elbow; in contrast, the gap criterion allows to identify the elbow location as the number of clusters with the largest gap.

The approach we propose here is based on the model originally proposed by [9], where, however, the authors considered the system operating with only three load levels, which are based on the concept of load duration curve. For this reason, we improved and extended the model in [9] so that each variable that describes the system operation has a value associated with the particular time interval chosen and the scenario, designated by the subscripts j and sc, respectively, $\forall j \in \psi^J$ and $\forall sc \in \psi^K$, as presented below.

3. Proposed MILP model

The approach we propose here aims at VVO considering chronological operation scenarios of demand and DERs. Thus, we consider the optimal operation of the available VVC devices, with the current control of automatic CBs and the voltage reference of VRs being explicit in the formulation.

3.1. Objective function

From the utility perspective, the objective function consists of minimizing the operation costs of PDS. Then, the costs of energy losses and the penalty costs for violating voltage limits constitute the objective function of our VVO problem, expressed by:

$$C^{\text{oper}} = \sum_{sc \in \psi^K} \Delta T_{sc} \left[C^{\text{loss}}_{sc} + C^{\text{vio}}_{sc} \right], \tag{1}$$

$$C^{\text{loss}}_{sc} = C^{\text{kWh}} S_{base} \sum_{j \in \psi^J} \Delta T_j \sum_{km \in \psi^B} p^{\text{loss}}_{km,j,sc}, \tag{2}$$

$$C^{\text{vio}}_{sc} = CV \sum_{j \in \psi^J} \sum_{m \in \psi^D} z_{m,j,sc}. \tag{3}$$

The annual operation costs are given by (1), where C^{loss}_{sc} represent costs of the energy losses and C^{vio}_{sc} the penalty costs of voltage violations, both costs calculated for the scenario sc. Note that the costs in (1) are multiplied by the scenario duration (ΔT_{sc}), which is obtained through K-means clustering. In (2), the term $p^{\text{loss}}_{km,j,sc}$ represents power losses in the branch km at time interval j of scenario sc, and it is estimated through the linear expressions detailed in [8]. Note that power losses are converted into energy losses by multiplying the term $p^{\text{loss}}_{km,j,sc}$ by the time interval duration (ΔT_j), calculated through $\Delta T_j = \frac{24}{J}$. Additionally, to address the voltage regulation, the costs of voltage violation of each scenario are calculated by (3). Thus, we adopted a formulation based on that defined in [9], where the strategy used to keep the voltage within limits aims at minimizing the voltage violations occurring at all nodes with load during each time interval.

3.2. Constraints

The objective function is subjected to the operational limits of the network and VVC devices, including fixed and automatic CBs, and VRs, $\forall j \in \psi^J$ and $\forall sc \in \psi^K$, as following presented.

3.2.1. Network constraints

The balance of currents is one of the constraints that describe the steady-state operation of a PDS during each time interval; this balance is obtained from the application of Kirchhoff's Current Law and expressed as:

$$\mathbf{S}\mathbf{f}^{\text{Re}}_{j,sc} + \mathbf{g}^{\text{Re}}_{j,sc} = \mathbf{d}^{\text{Re}}_{j,sc} + \Delta\mathbf{f}^{\text{Re}}_{j,sc}, \tag{4}$$

$$-\mathbf{q}^{A}_{j,sc} + \mathbf{S}\mathbf{f}^{\text{Im}}_{j,sc} + \mathbf{g}^{\text{Im}}_{j,sc} = \mathbf{d}^{\text{Im}}_{j,sc} + \Delta\mathbf{f}^{\text{Im}}_{j,sc}. \tag{5}$$

The CBs are modeled as constant impedance and $\mathbf{q}^{A}_{j,sc}$ represents the vector of current injections of automatic CBs, obtained for all nodes with CB ($\forall m \in \psi^{CB}$) through the disjunctive formulation proposed by [8]. On

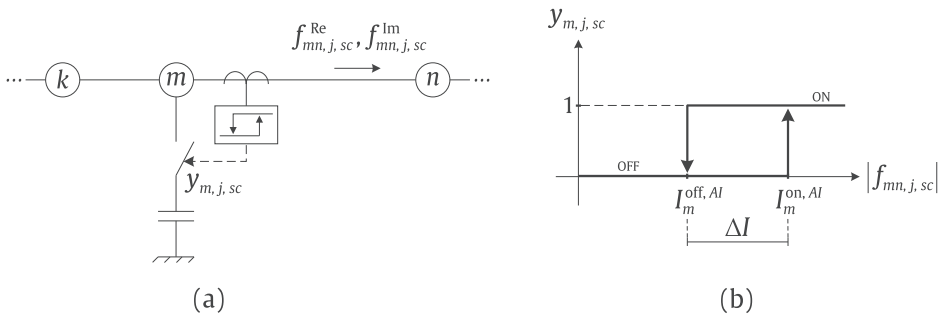

Fig. 2. Current control of automatic CBs: (a) system with a capacitor bank at the bus *m*; (b) current hysteresis control.

the other hand, the loads are represented through constant current injections [33], and the terms $\mathbf{d}^{Re}_{j,sc}$ and $\mathbf{d}^{Im}_{j,sc}$ represent the real and imaginary parts of the current injection in all nodes with load ($\forall m \in \psi^D$). In accordance to the available operation modes of DERs, except for the slack node, all nodes with generation capacity are assumed to operate as a PQ bus. In doing so the current injections of DERs ($\mathbf{g}^{Re}_{j,sc}$ and $\mathbf{g}^{Im}_{j,sc}$) are obtained through the clustering step and represent the chronological operation of each DER. Additionally, a compensation current is calculated exclusively for the VR terminal node ($\forall m \in \psi^{VR}$), and the vectors of change in the current flows upstream of VRs are represented by $\Delta\mathbf{f}^{Re}_{j,sc}$ and $\Delta\mathbf{f}^{Im}_{j,sc}$. To handle the nonlinearities arising in our formulation, we used the disjunctive formulation thoroughly detailed in [9].

The application of the Kirchhoff's Voltage Law, in turn, allows to calculate the voltage drops in all branches ($\forall km \in \psi^B$), as follows:

$$K_{km,j,sc}R_{km}f^{Re}_{km,j,sc} - X_{km}f^{Im}_{km,j,sc} + [\mathbf{S}']_{line\ \ km}\mathbf{V}_{j,sc} - \Delta V_{m,j,sc} = 0. \quad (6)$$

Due to presence of VRs, (6) also considers the change in voltage ($\Delta V_{m,j,sc}$) $\forall m \in \psi^{VR}$. Besides, similar to $\Delta\mathbf{f}^{Re}_{j,sc}$ and $\Delta\mathbf{f}^{Im}_{j,sc}$, given the nonlinear relationships involving the determination of $\Delta V_{m,j,sc}$, we represent this term using the disjunctive linearization defined in [9]. Additionally, to better approximate the solution obtained with our model to the exact solution obtained with power flow calculation, we adopted the adjustment factor $K_{km,j,sc}$ ($\forall km \in \psi^B$), as described in [8].

3.2.2. Volt-var control

A very common characteristic of VVO problems, it is the assumption of a central control designed to simultaneously coordinate all volt-var devices according to a system-wide objective. Although this type of control can be considered in expansion planning studies to forecast some operational modes, it is impossible to contemplate all possibilities. Thus, when the system operates under a situation not foreseen in the model, it would be necessary to run an optimal power flow to determine the required adjustments of the model.

The problem described above can become worse if we consider that duration of the unforeseen conditions is unknown; therefore, numerous adjustments may be applied only for a short time. In addition, to avoid an intermittent operation, many VVC devices are programmed to delay their operation, which is implemented through thresholds and also hysteresis in their control. Consequently, if the model neglects these characteristics, it can result that the VVC do operate properly.

For this reason, we have included a local control of CBs and VRs in our model. Besides, the electrical quantities used in the VVO (such as branch current to set the control of CBs and node voltage to adjust VRs), also affect the cost of energy losses and the penalty costs of voltage violations, thus influencing the global optimum solution. In the following, we address the VVC of automatic CBs and VRs with line drop compensation.

a. *Capacitor bank*

The proposed scenario approach reduces the number of scenarios while maintaining the correlation among different quantities (loads and DERs). However, the typical days resulting from the K-means clustering are not in an appropriate sequence. Therefore, a single rule, valid for all scenarios, is required to define the operation mode of automatic shunt CBs. In this respect, we propose a novel MILP formulation for current control of automatic shunt CBs; as required, this formulation is sensitive to the downstream load variation of all scenarios. Essentially, the CB control monitors the downstream branch current ($f^{Re}_{mn,j,sc}, f^{Im}_{mn,j,sc}$) and switches the CB on or off based on a current hysteresis controller, as depicted in Fig. 2.

We propose a linear disjunctive model to optimally adjust the on-off currents, $I^{on,AI}_m$ and $I^{off,AI}_m$ ($\forall m \in \psi^{CB}$) (see Fig. 2(b)), as follows:

$$I^{trs,AI}_{m,j,sc} - I^{on,AI}_m \leqslant M y^{AI}_{m,j-1,sc}, \quad (7)$$

$$I^{on,AI}_m - I^{trs,AI}_{m,j,sc} \leqslant M y^{AI}_{m,j-1,sc}, \quad (8)$$

$$I^{trs,AI}_{m,j,sc} - I^{off,AI}_m \leqslant M\left(1 - y^{AI}_{m,j-1,sc}\right), \quad (9)$$

$$I^{off,AI}_m - I^{trs,AI}_{m,j,sc} \leqslant M\left(1 - y^{AI}_{m,j-1,sc}\right), \quad (10)$$

$$I^{off,AI}_m + \Delta I \leqslant I^{on,AI}_m. \quad (11)$$

According to the control strategy adopted, each capacitor is switched on when the transition current $I^{trs,AI}_{m,j,sc}$ is greater than $I^{on,AI}_m$ in (7) and (8). Further, note that each CB is switched on only if the CB remained in the off state during the preceding time interval ($y^{AI}_{m,j-1,sc} = 0$). In contrast, if the current $I^{trs,AI}_{m,j,sc}$ is below the limit given by $I^{off,AI}_m$ in (9) and (10), the corresponding automatic CB is switched off only if the CB remained in the on state during the preceding time interval ($y^{AI}_{m,j-1,sc} = 1$). The current hysteresis controller is defined considering a bandwidth ΔI in order to represent the current excursion between the prescribed limits, illustrated in Fig. 2 (b). The transition current $I^{trs,AI}_{m,j,sc}$ is calculated based on the magnitude of the monitored downstream branch current $|f_{mn,j,sc}|$ as follows:

$$|f_{mn,j,sc}| - I^{trs,AI}_{m,j,sc} \leqslant M y^{AI}_{m,j,sc}, \quad (12)$$

$$I^{trs,AI}_{m,j,sc} - |f_{mn,j,sc}| \leqslant M\left(1 - y^{AI}_{m,j,sc}\right). \quad (13)$$

In order to obtain $|f_{mn,j,sc}|$ through a linearized formulation, we propose a piecewise linear, bivariate mixed-integer function to approximate $|f_{mn,j,sc}|$, as detailed in Appendix A. Besides, we highlight that M is a number big enough to satisfy the possible values of $|f_{mn,j,sc}|$ and $I^{trs,AI}_{m,j,sc}$.

Finally, the limits of daily switching of CBs are expressed by:

$$w^{AI}_{m,j,sc} \geqslant y^{AI}_{m,j,sc} - y^{AI}_{m,j-1,sc}, \quad (14)$$

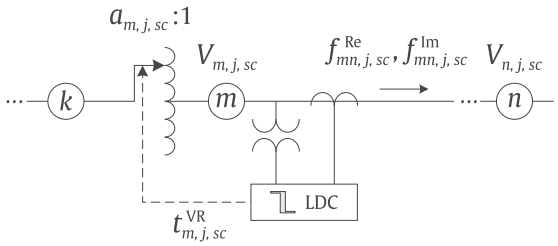

Fig. 3. Simplified circuit representing the tap changing of a VR with LDC.

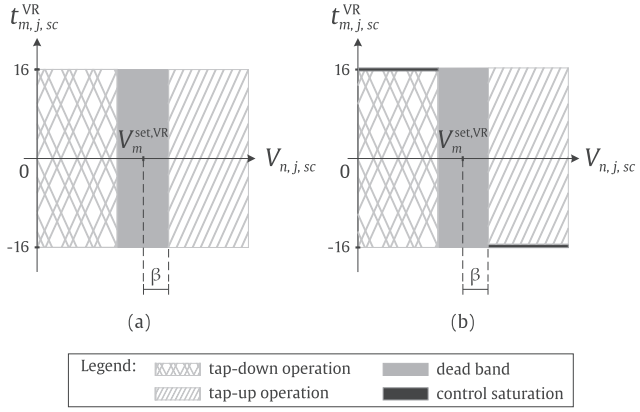

Fig. 4. Tap operation control: (a) approach without control saturation; (b) proposed approach considering saturation.

$$w^{AI}_{m,j,sc} \geqslant y^{AI}_{m,j-1,sc} - y^{AI}_{m,j,sc}, \tag{15}$$

$$W^{max,AI}_{m,sc} \geqslant \sum_{j=2}^{24} w^{AI}_{m,j,sc}. \tag{16}$$

b. *Voltage regulator*

The main extensions and contributions of the proposed VR control concerning the model developed by [9] are: (i) the formulation of a VR control with LDC; (ii) the voltage reference, to be held at the output of a given VR, is no longer a parameter but a continuous variable in the proposed MILP model; (iii) the inclusion of a model to determine the optimal regulation range of VRs based on operation limits of the controller; (iv) the introduction of a regulation zone including saturation in the VR control, so that the taps of each device can be changed under specific operational conditions.

In this paper, the changing of taps of each VR is controlled by the LDC. A simplified circuit of a LDC is depicted in Fig. 3, showing how it is connected to the feeder through a potential transformer and a current transformer. Essentially, the LDC estimates the voltage on a specified node n, providing information to change the tap position ($t^{VR}_{m,j,sc}$) in order to regulate the voltage when the load changes. Furthermore, since this method considers the downstream current flow ($f^{Re}_{mn,j,sc}$,$f^{Im}_{mn,j,sc}$), the VR control becomes able to track load variations.

The tap position of a VR installed at the node m is represented through an integer variable $t^{VR}_{m,j,sc}$, which is obtained from [9]:

$$t^{VR}_{m,j,sc} = \sum_{i=1}^{6} 2^{(i-1)} r_{i,m,j,sc} - 16, \tag{17}$$

where $r_{i,m,j,sc}$ is a binary variable related to the constraint $\sum_{i=1}^{6} 2^{(i-1)} r_{i,m,j,sc} \leqslant 32$. VRs can be connected in two ways, named Type A and Type B connection, with the Type B being more common [34]. Then, assuming a VR with Type B connection, the transformation ratio for node $m \in \psi^{VR}$ is given by:

$$a_{m,j,sc} = 1 - 0.00625 t^{VR}_{m,j,sc}, \tag{18}$$

where $t^{VR}_{m,j,sc}$ varies inside the interval [-16,16], as shown in Fig. 4 (a), and $a_{m,j,sc}$ inside the interval $[(1-10\%), (1+10\%)]$ in discrete steps of 0.625%. In this way, the voltage reference ($V^{set,VR}_m$) is maintained at the output of a given VR within the regulation range of ±10%.

Note that the tap position changes only when $V_{n,j,sc}$ leaves the dead band of the controller, as depicted in Fig. 4. The dead band limits are defined by the VR bandwidth, called β. Thus, the allowed excursion of the regulated voltage ($V_{n,j,sc}$) regarding the reference voltage $V^{set,VR}_m$ ($\forall m \in \psi^{VR}$) is given by:

$$V^{set,VR}_m - \beta \leqslant V_{n,j,sc} \leqslant V^{set,VR}_m + \beta, \tag{19}$$

where the term $V^{set,VR}_m$ is a continuous variable which represents the optimal adjustment of the VR at node m. However, if the interval ± 10% is adopted, as proposed by [9], it may be impossible to regulate the voltage for all time intervals j and scenarios sc, thus limiting the VR control operation. In this situation the VR control reaches saturation and it is no longer possible to impose $V^{set,VR}_m$, as depicted in Fig. 4 (b). In such a case, the VR operates at the limit reached during this period (−10% or + 10%), without regulating the voltage at this specific operation condition. As a result, two situations can occur: (a) the first one is common during overload-periods (peak hours) when the VR needs to elevate the secondary voltage to adjust the voltage at the regulated node; (b) the second one takes place when the VR needs to reduce the secondary voltage to adjust the voltage of the regulated node so that it comes into the operating range. Both situations require changing the traditional approach of tap operation control, as shown in Fig. 4 (b).

Therefore, to handle the first situation, we propose to include an additional term on the right side of expression (19):

$$V_{n,j,sc} - \left(V^{set,VR}_m - \beta\right) \geqslant -M r_{6,m,j,sc}. \tag{20}$$

With the additional term, when the VR operates with maximum tap (+16), the constraint which forces the regulated voltage to be greater than the reference voltage is relaxed. It is worth mentioning that, based on expression (17), operation with maximum tap implies $r_{6,m,j,sc} = 1$, for all other tap positions $r_{6,m,j,sc} = 0$. Besides, we highlight that M is a number sufficiently large to allow all possible values of $V_{n,j,sc}$ and $V^{set,VR}_m$. Additionally, the second situation implies:

$$V_{n,j,sc} - \left(V^{set,VR}_m + \beta\right) \leqslant M\left(1 - rr_{m,j,sc}\right), \tag{21}$$

where $rr_{m,j,sc}$ is a binary variable which becomes null only when the minimum tap (–16) is selected, i.e. only when all variables $r_{i,m,j,sc}$ are null for a particular time interval j and scenario sc. The variable $rr_{m,j,sc}$ is then defined by:

$$0 \leqslant rr_{m,j,sc} \leqslant 1, \tag{22}$$

$$rr_{m,j,sc} \leqslant \sum_{i=1}^{6} r_{i,m,j,sc}, \tag{23}$$

$$rr_{m,j,sc} \geqslant r_{i,m,j,sc}, \quad \forall i = \{1,2,\ldots,6\}. \tag{24}$$

The formulation expressed by (20)–(24) allows solving the proposed MILP model for VR control considering control saturation; it also makes it possible to change taps and find solutions for the VVO problem. Further, numerical results addressed later will make clearer not only the impact but also the functionally of the VR control with saturation (see Fig. 13).

Finally, the limits of daily switching of taps are expressed by:

$$w^{VR}_{m,j,sc} \geqslant t^{VR}_{m,j,sc} - t^{VR}_{m-1,j,sc}, \tag{25}$$

Table 1
Summary of the proposed MILP.

Equation number	Main Variables	Equation type	Description
(1)	C^{oper}	objective function	annual operation cost
(2)	C_{sc}^{loss}	objective function	energy losses cost
(C.3)–(C.5)	$P_{km,j,sc}^{loss}$	objective function	power losses
(3)	C_{sc}^{vio}	objective function	voltage violation cost
(B.2)–(Appendix B)	z	objective function	annual voltage violation
(4) and (5)	$\mathbf{I}_{j,sc}^{Re}, \mathbf{I}_{j,sc}^{Im}$	network constraints	Kirchhoff's Current Law
(6)	$\mathbf{V}_{j,sc}$	network constraints	Kirchhoff's Voltage Law
(7)–(13)	$y_{m,j,sc}^{AI}, I_{m}^{on,AI}, I_{m}^{off,AI}$	VVC constraints	CB current control
(14)–(16)	$w_{m,j,sc}^{AI}$	VVC constraints	limits for the daily switching of CBs
(17)–(24)	$V_{m}^{set,VR}, t_{m,j,sc}^{VR}$	VVC constraints	VR control
(25)–(27)	$w_{m,j,sc}^{VR}$	VVC constraints	limits for the daily operation of VR taps

Table 2
Comparison of our approach with that in [9].

Aspect		Ref. [9]	Proposed approach
Load modeling	operation mode	load duration curve	chronological scenarios
	power factor	constant	variable
DER modeling	operation mode	power factor range	constant power
	power injection	constant	variable
	power factor	variable	constant
VVO formulation	CB control	load level	current
	VR control	without LDC	with LDC
	daily switching limits of VVC devices	no	yes
	VR operation with saturation	no	yes

$$w_{m,j,sc}^{VR} \geq t_{m-1,j,sc}^{VR} - t_{m,j,sc}^{VR}, \tag{26}$$

$$W_{m,sc}^{max,VR} \geq \sum_{j=2}^{24} w_{m,j,sc}^{VR} \tag{27}$$

where $W_{m,sc}^{max,VR}$ is the daily limit to operate the VR taps.

3.3. Summary of the proposed MILP model

Table 1 summarizes all variables and main mathematical expressions of the proposed MILP model, highlighting the variables and the type of function (objective function, network constraints or VVC constraints); this table also includes a short description of each group of expressions.

The formulation of proposed MILP model, summarized in Table 1, is considered new by the following aspects:

1. the definition and use of a MILP model for volt-var optimization including the chronology of operation and inherent simultaneity of multiple loads and DERs;
2. the formulation of a comprehensive MILP model for volt-var optimization, which includes (i) explicit control variables to turn on/off automatic CBs and (ii) explicit VR adjustment by including the possibility of line drop compensators;
3. the possibility to limit the daily switching of CBs and/or the daily operation of VR taps;
4. the use of electrical quantities to model volt-var control devices, thus allowing to design more realistic control strategies;
5. the development of a representation that allows the operation of automatic CBs to be sensitive to variations in downstream currents, based on a current control with hysteresis;
6. the model of VR control remains feasible, since it accounts for the possibility of saturation under certain operating conditions.

3.4. Comparison with a similar model

As already stated, the proposed VVO model is an extension of the MILP model described in [9], which essentially addressed the problem of PDS expansion planning. Nevertheless, some operation aspects were also included in the objective function defined in [9]. Thus this section discusses some aspects common to both approaches, which are resumed in Table 2.

Concerning load modeling aspects, the most common way to represent the load demand is through loading levels determined from load duration curves. Thus, [9] used three loading levels (heavy, medium, and light) to represent the load during a year. However, this approach disregards the chronological operation of the system, since the same simultaneous behavior was assumed for all loads. By contrast, the approach we propose here considers the simultaneity and chronological combination of all loads through 24-hours scenarios. For example, with three scenarios, the proposed approach can represent up to 72 levels of power for each loaded node. Besides, while the power factor is constant in [9], in the proposed approach the power factor can vary during the system operation.

Regarding the DER modeling, [9] assumed generators operating with constant power injection and variable power factor. On the other hand, here we modeled DER units through a combination of solar PV and wind generators, while the chronological operation is represented by 24-hours scenarios. For example, assuming three scenarios of 24-hours, the proposed model can represent the DER operation using 72 values of power injection.

Furthermore, when the load variation is represented by three load levels, it is possible to adapt the operation of CBs to each load level and also define adequate VR taps, as proposed by [9]. However, the flexibility of load modeling offered by the proposed approach makes it possible to design a CB control based on the effective feeder loading. Moreover, the LDC formulation makes the VR control sensitive to downstream load variations, so that electrical quantities must be used to model VVC. Further, the proposed approach considers daily switching limits for VVC devices. In contrast to [9], here the VR control includes saturation in the regulation zone so that the VR taps can be adjusted to any operating conditions. Note that without saturation, the problem would become infeasible due to the inability of VVC devices to regulate the voltage using maximum or minimum taps.

4. Implementation steps

The proposed MILP model for operation planning of PDS involves several steps, since different methods are used to obtain the final solution. Thus, an overview diagram is depicted in Fig. 5, showing the internal logic along with the main steps and methods used to solve the VVO problem.

Initially, the scope of operation planning depends on the particular case under consideration (see **step 1** in Fig. 5). Each case study presents its particularities, according to network characteristics and VCC devices.

According to **step 2** of Fig. 5, to preserve the simultaneity and chronological combination of different loads and DERs, including both real and reactive power demands, typical scenarios are clustered with a

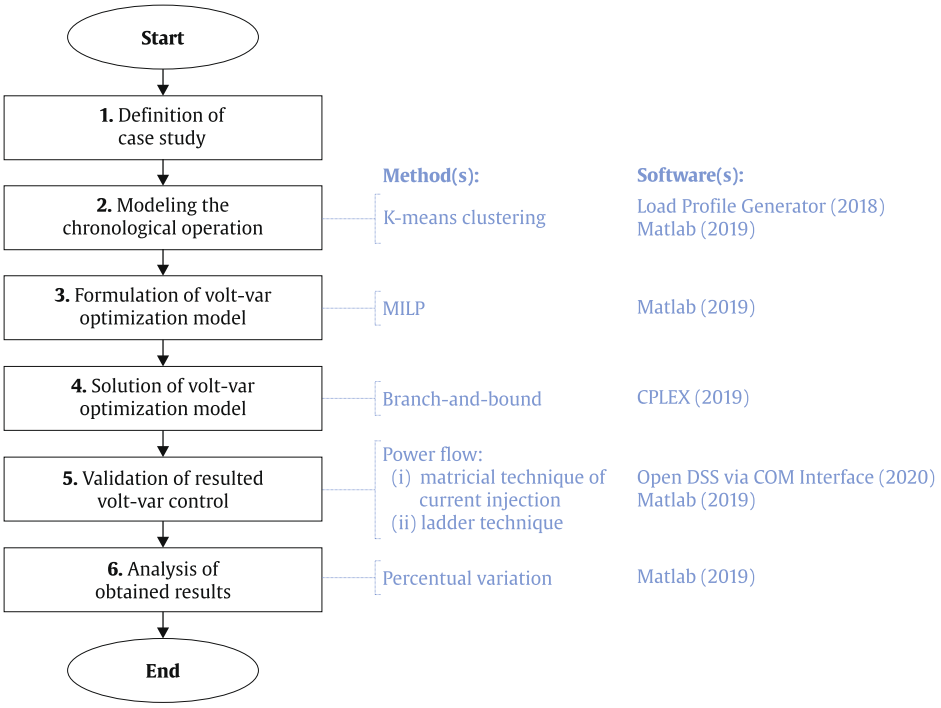

Fig. 5. Overview diagram of the proposed strategy to solve VVO.

K-means algorithm as described in Section 2. In cases where load profiles and DER generation curves are not available, it is possible to simulate the full operation (365 days) of 24-hours profiles for all loads of each system using the Load Profile Generator software [35]; it is also possible to use data from databases through the internet to represent the DER behavior [36,37].

In **step 3** of Fig. 5, the proposed MILP model, described by expressions (1)–(24), was coded using optimization programming language [38] and implemented in the software Matlab®. Further, in **step 4**, the MILP is solved by the solver CPLEX® [39] using default options. The optimality gap (relative MIP gap tolerance) was chosen as 10^{-4}, which means that CPLEX stops when a feasible integer solution becomes very close to the optimal solution (difference of about 0.01%). The absolute MIP gap tolerance is 1E-6, meaning that when the gap between the best integer objective and the objective of the best node remaining falls below 1E-6, the solver finishes the search for solutions. Besides, we used the following hardware: Intel® Core™, i5-3337U CPU @ 1.80 GHz processor, 8 GB RAM, and Windows 10 Pro 64-bit. The optimal solutions are obtained including: (i) total operation costs; (ii) annual power losses; (iii) annual voltage violations; (iv) voltage level to be held by VRs (if applicable); and (v) the current control that switch automatic CBs on and off (if applicable).

The **step 5** of Fig. 5 consists of checking and validating the results obtained against results obtained with other methods. In the practical

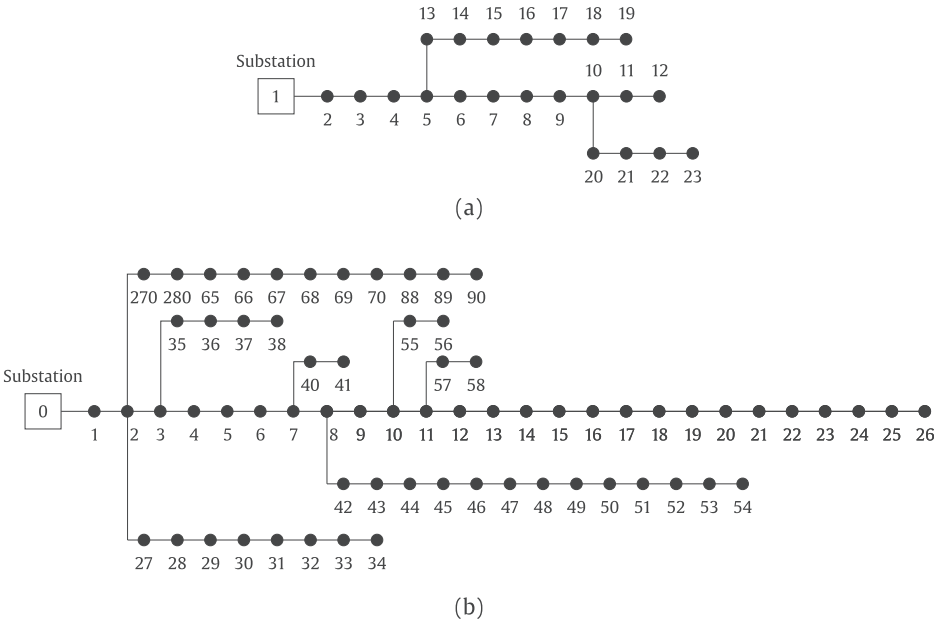

Fig. 6. PDS used to test and validate the model: (a) 23-node system; (b) 69-node system.

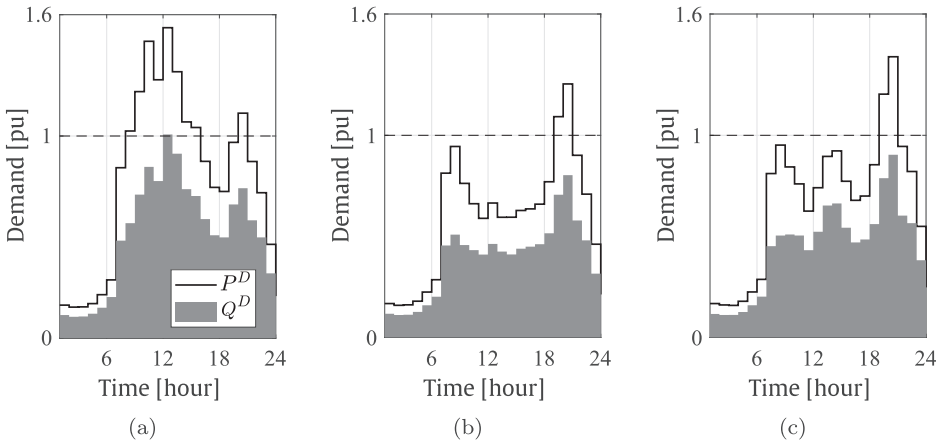

Fig. 7. Aggregated loadshape of active (P^D) and reactive power (Q^D) demands at the substation of the 23-node system ($S_{base} = 4$ MVA) during (a) scenario 1, (b) scenario 2, and (c) scenario 3.

case studies reported here, the operation points were determined with the linearized model and subsequently compared with those operation points obtained through nonlinear power flow. For the case studies that include VVC devices, we executed the power flow considering the MILP optimal solution of current control of CBs and/or VR tap control. Then, the power flow was modeled and executed in OpenDSS software [40] via COM interface using MATLAB® [41].

Finally, the **step 6** of Fig. 5 consists of analyzing the performance of the proposed MILP model, considering the results obtained in the previous steps.

The steps thus far described contain the main novelties of the proposed solution technique. In the next section, we present and analyze practical results obtained for VVO of three different PDS.

5. Numerical results

We assessed the validity and performance of the proposed MILP model using results obtained from tests of a 23-node [42] and 69-node [43] distribution systems. Further, we also present a further application example consisting of a real distribution system with 733 nodes [8]. According to the proposed VVO approach, the optimal operation of CBs and VRs can be solved independently, or integrated into the same test, thus resulting in the following test combinations:

- *Base Case*: optimal operation of PDS without voltage regulation devices (CB, VR, or DER);
- *CB*: optimal operation of PDS considering installed CBs only;
- *VR*: optimal operation of PDS considering installed VRs only;
- *CB* + *VR*: optimal operation of CBs and VRs;
- *Base Case* + *DER*: optimal operation of PDS considering installed DER only;
- *CB* + *DER*: optimal operation of PDS considering installed CBs and DER;
- *VR* + *DER*: optimal operation of PDS considering installed VRs and DER;
- *CB* + *VR* + *DER*: optimal operation of PDS considering installed CBs, VRs, and DER.

In the next subsections we present and discuss the main results regarding the practical tests.

5.1. Simulated case studies

To evaluate the method we proposed thus far, it was applied to the two distribution systems depicted in Fig. 6. The first system contains 23 nodes and operates with 13.8 kV and 60 Hz, as illustrated in Fig. 6 (a); further, each branch is 2 km long and the nominal load, approximately 4158 kW and 2728 kvar, is evenly distributed among the nodes 2–23 [42]. The second system has 69 nodes and operates with 12.66 kV, with the nominal load of 4027 kW and 2796 kvar being distributed among 48 nodes [43].

The placement of CBs and VRs in each system studied was based on the optimal allocation solution of expansion planning of PDS proposed by [10]. Three different types of CBs were considered: fixed CB of 600 kvar, automatic CB (switched type) of 600 kvar, and automatic CB of 1200 kvar as maximum nominal power. Besides, we used VRs with maximum current of 400 A, a regulation range of ±10%, and a bandwidth of ±1% ($\beta = 0.01$). Furthermore, the voltage at the substation was fixed at 1.02 pu for all tests in both systems. Finally, we assumed 0.11 US $/kWh as energy cost, 10 US$/h as linear penalty factor for voltage violations, and $[0.975, 1.05]$ pu as the interval for voltage limits of loaded nodes [10].

5.1.1. Chronological operation

To preserve the simultaneity and chronological combination of different loads and DERs, including both real and reactive power demands, a set of typical scenarios were clustered with a K-means algorithm (as described in Section 2). Originally, no data were available regarding the hourly variation of the load (loadshape) of both systems. Therefore, as no real data were available, we simulated the full operation (365 days) of 24-hours profiles for all loads of each system using the Load Profile Generator software [35]. The data thus obtained were then used in the tests.

We highlight that the proposed MILP model is valid for any time horizon. Therefore, as long as forecast data are available, the formulation presented in the paper is fully applicable to short (one day) as well as to long time horizon (one year). For the case studies involving the chronological operation of PDS discussed in the paper, we chose one year as the optimization horizon because the scenarios selected through the K-means clustering algorithm proved to be sufficient to describe the PDS yearly operation.

Since the original systems tested do not consider installed DERs, a DER unit was connected to the node 14 in the 23-node system and node 20 in the 69-node system. Each DER unit has 1 MW as the maximum capacity of active power generation and power factor of 1.0. Moreover, the curve of the power generated by the DER unit is a combination of two different sources, 500 kW coming from solar PV and 500 kW from wind generation, obtained using Renewables Ninja dataset [36,37].

Based on the elbow criteria, the case studies require at least 2 scenarios to accurately represent their chronological operation. In this way, considering the sensibility analysis of clustering thoroughly explained in [31], we adopted three scenarios for both systems. Fig. 7 depicts the

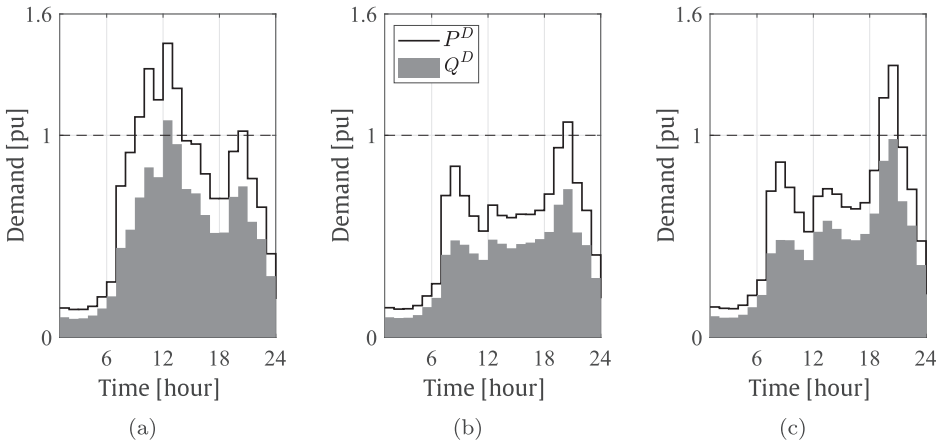

Fig. 8. Aggregated loadshape of active (P^D) and reactive power (Q^D) demands at the substation of the 69-node system ($S_{base} = 4$ MVA) during (a) scenario 1, (b) scenario 2, and (c) scenario 3.

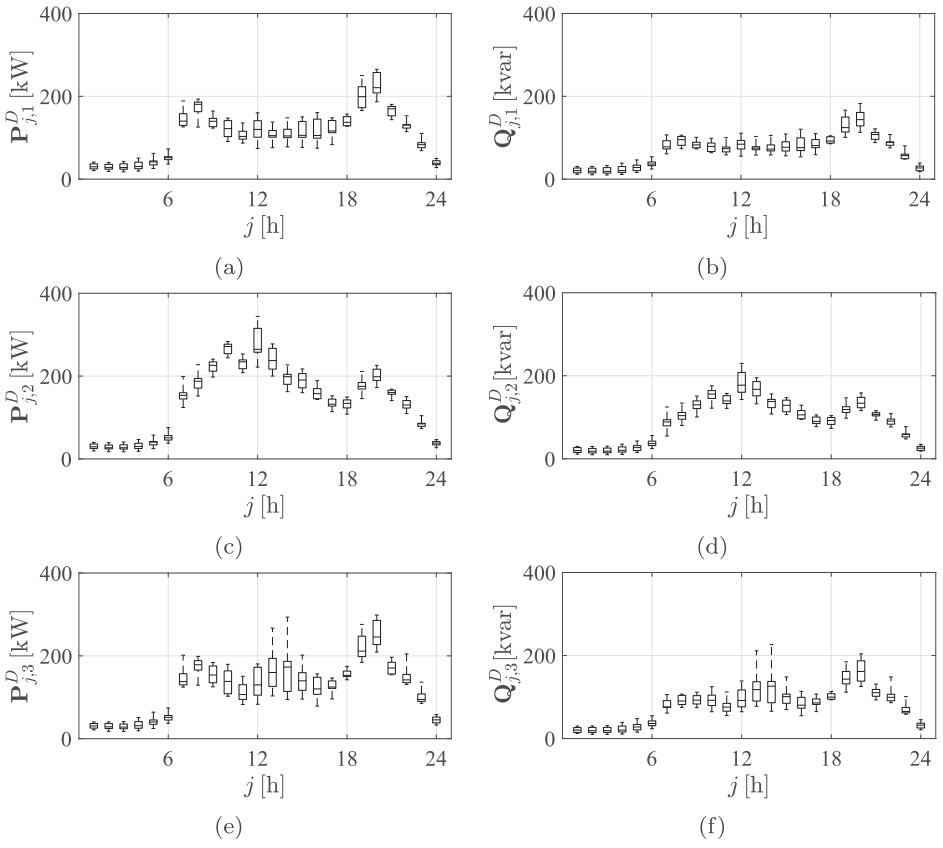

Fig. 9. Boxplot of hourly active and reactive power demands of all loads of the 23-node system during (a)-(b) scenario 1, (c)-(d) scenario 2, and (e)-(f) scenario 3.

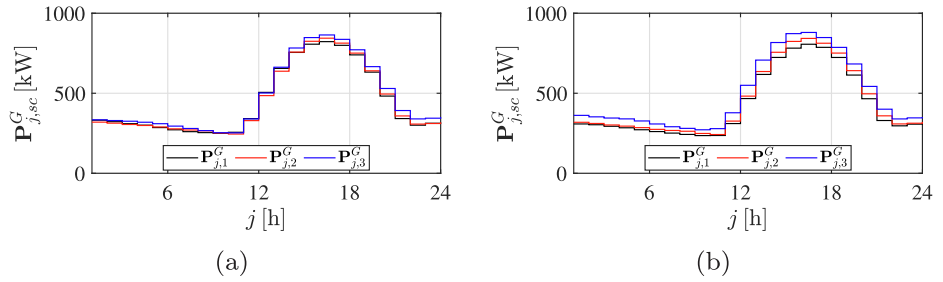

Fig. 10. Generation curves of DER for (a) the 23-node system and (b) the 69-node system.

Table 3
Scenario duration.

System	Occurrence (ΔT_{sc}) [days/year]		
	$sc = 1$	$sc = 2$	$sc = 3$
23-node	110	148	107
69-node	112	135	118

Table 4
Summary of the MILP results for the 23-node system.

Test	C^{oper} [$\times 10^3$ US$]	Losses [MWh]	z [pu]	Processing time [s]
Base Case	212.94 (−0.45%)[a]	1380.63 (−0.61%) [b]	0.6971 (−0.0002)[c]	21
CB	124.45 (−1.04%)	1059.30 (−0.38%)	0.0904 (−0.0098)	115
VR	177.66 (0.36%)	1564.31 (2.37%)	0.0637 (−0.0382)	529
CB + VR	123.99 (−1.41%)	1112.96 (−0.13%)	0.0178 (−0.0183)	3360
Base Case DER	184.38 (0.28%)	1185.44 (0.13%)	0.6162 (0.0040)	23
CB + DER	100.71 (−0.84%)	865.23 (−0.08%)	0.0631 (−0.0089)	103
VR + DER	145.54 (−3.24%)	1292.20 (−1.56%)	0.0387 (−0.0299)	572
CB + VR + DER	98.52 (−3.06%)	888.50 (−1.41%)	0.0090 (−0.0195)	1564

[a] Percentual difference of operational costs in relation to power flow result.
[b] Percentual difference of power losses in relation to power flow result.
[c] Per unit difference of voltage violations in relation to power flow result.

Table 5
Summary of VVC results for the 23-node system.

Test	Capacitor Bank				Voltage Regulator	
	Node	Type	$I_m^{on,AI}$ [pu]	$I_m^{off,AI}$ [pu]	Node	$V_m^{set,VR}$ [pu]
Base Case	–	–	–	–	–	–
CB	8	A1200	1.4208	1.2007	–	–
	9	F600	–	–		
	16	F600	–	–		
	21	A600	0.3434	0.2213		
VR	–	–	–	–	5	1.0156
CB + VR	8	F600	–	–	5	1.0069
	16	F600	–	–		
	21	A600	0.3146	0.1950		
Base Case DER	–	–	–	–	–	–
CB + DER	8	A1200	1.4231	1.2028	–	–
	9	F600	–	–		
	16	F600	–	–		
	21	A600	0.3441	0.2219		
VR + DER	–	–	–	–	5	1.0280
CB + VR + DER	8	F600	–	–	5	1.0100
	16	F600	–	–		
	21	A600	0.3441	0.2219		

profile of aggregated load demands at the substation of the 23-node system during each scenario, while Fig. 8 depicts the scenario profiles at the substation node of the 69-node system.

According to the model proposed here, every load presents a different loadshape during each scenario. Take the case of time-variable behavior of the loads of the 23-node system, illustrated in Fig. 9, where each boxplot illustrates the vector of active ($\mathbf{P}^D_{j,sc}$) or reactive power demand ($\mathbf{Q}^D_{j,sc}$) during hour j and scenario sc. Although all 22 loads of the 23-node system have the same nominal power (189 kW and 124 kvar), they assume a different variation with the time, as shown by the hourly variation of each scenario. Note that scenario 3 has the largest power variation, as illustrated by Fig. 9 (e)-(f).

In relation to the chronological operation of the DER units, the maximum generation occurs at 4 pm and corresponds to 864.26 kW for the 23-node system and 879.91 kW for the 69-node system. The DER generation curve of each scenario is depicted in Fig. 10. Finally, Table 3 shows the scenarios duration (days/year) of each system.

5.2. Results for the 23-node system

The test results for the 23-node system are shown in Table 4, including the Base Case (without CBs and VRs) and Base Case DER. Considering a one-year horizon, columns 2 to 5 of Table 4 show the results regarding, respectively, operation cost, energy losses, voltage violation and processing time; in this table, the annual voltage violation z is determined from the expression $z = \sum_{sc\in\Psi^K}\Delta T_{sc}\sum_{j\in\Psi^J}\sum_{m\in\Psi^D} z_{m,j,sc}$. Furthermore, Table 5 lists the placement (node) of VVC devices, as well as the resulting current control variables that switch automatic CBs on and off ($I_m^{on,AI}$ and $I_m^{off,AI}$), and voltage level to be held by VRs ($V_m^{set,VR}$).

The relative differences in parenthesis in Table 4 were calculated through power flow studies done for each case using the optimal parameters given in Table 5. For example, to evaluate the effectiveness of the VR control, the value of $V_m^{set,VR}$ of a given VR installed at node 5 was used in the power flow study of the 23-node system. For the nonlinear power flow we assumed CBs as 100% constant impedance; loads as 50% constant power, and 50% constant impedance; and DERs as 100% constant power [10].

A comparison between the operation costs calculated with the proposed MILP model and those obtained through power flow studies reveals a difference of only −3.24%, thus confirming the good performance of the VR control. Similarly, to evaluate the effectiveness of the CB control, the values of $I_m^{on,AI}$ and $I_m^{off,AI}$ of all automatic CBs determined with the proposed MILP model were also used in the power flow study. Further, the results of CB + DER Test show small errors in the energy losses and the voltage violations. Finally, we observed differences as low as −0.84% between the operation costs calculated with the proposed MILP model and nonlinear flow.

The VVO problem of the CB Test consisted of calculating the current necessary to switch the automatic CBs on and off. In this way, even with expressive hourly load variations of each scenario (illustrated in Fig. 9), the control selects only one value of current to switch the CB during the whole year. Fig. 11 illustrates $I_m^{on,AI}$ and $I_m^{off,AI}$ of the CB of 1200 kvar installed at the node 8. Note that, based on the monitored downstream branch current ($|f_{89,j,sc}|$) illustrated in Fig. 11 (a)-(c), the optimal solution indicated intermittent operations for the CB between on and off state, as depicted in Fig. 11 (d)-(f). Besides, this example shows that the daily switching limit imposed on the CBs by the constrains (14)–(16) was in fact respected. In addition, Fig. 11 (d)-(f) shows that the hours of operation of the CB obtained with the proposed MILP model is very close to those obtained with the nonlinear power flow. However, a small difference between the CB operation determined through both methods can be observed towards the end of scenario 3, as depicted in Fig. 11 (f); according to the power flow, the CB should stay on an hour longer. Finally, the CB Test exhibits an expressive reduction in the voltage violations when compared with the Base Case, as well as a decrease in the energy losses.

Concerning the VVO problem of the VR Test, the goal is to find the voltage reference ($V_m^{set,VR}$) to be held at the output of a VR installed at node 5. Considering an LDC, the VR control adjusts the taps to regulate the voltage of node 6 ($V_{6,j,sc}$). Fig. 12 (a)-(c) depicts the voltage profile of $V_{6,j,sc}$ for all scenarios, where it is possible to recognize that only one value exists for $V_m^{set,VR}$. The tap positions indicated by the proposed MILP model along with those indicated by the power flow study are both illustrated in Fig. 12 (d)-(f). This test highlights the importance of a VR control strategy including saturation within the regulation zone during

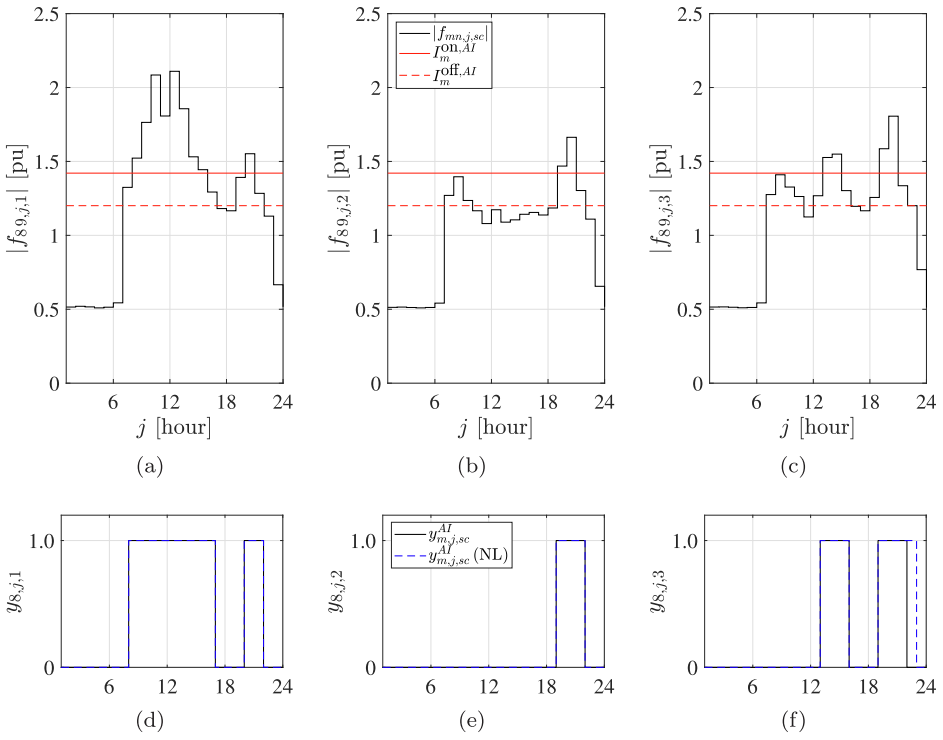

Fig. 11. Results obtained with a controlled CB at node 8 for the 23-node system in CB Test: (a)-(c) hourly levels of monitored downstream branch current during scenarios 1, 2, and 3, respectively; (d)-(f) hourly CB state during scenarios 1, 2, and 3, respectively.

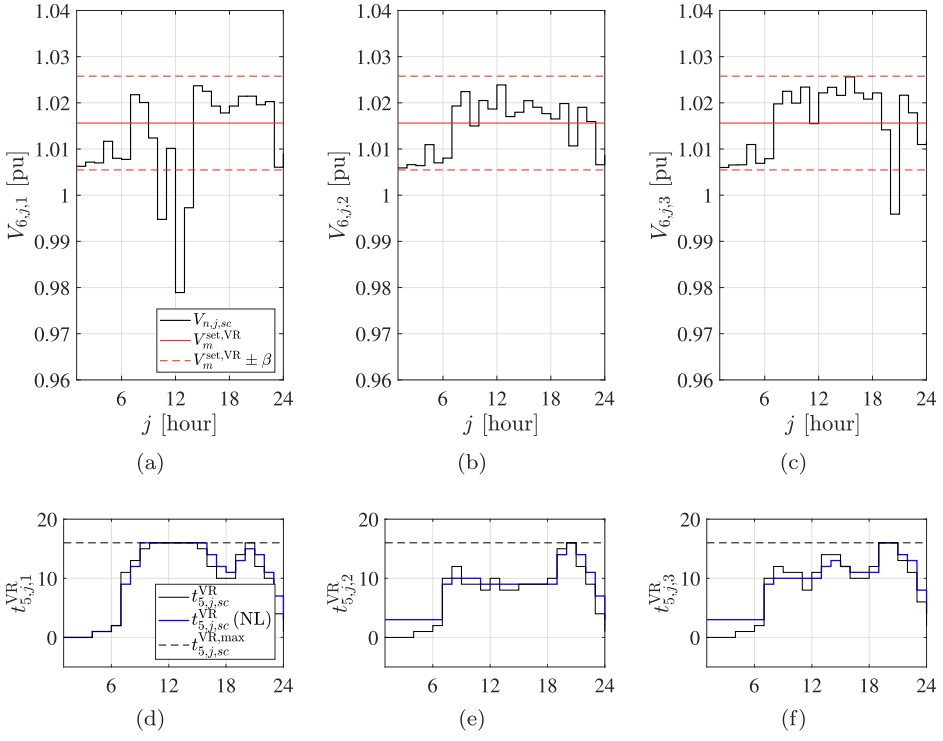

Fig. 12. Results obtained for a controlled VR at node 5 of the 23-node system for VR Test: (a)-(c) hourly voltage levels of remote node 6 during scenarios 1, 2, and 3, respectively; (d)-(f) hourly taps during scenarios 1, 2, and 3, respectively.

peak load periods, as expressed by (20)–(24). To better illustrate this aspect, Fig. 13 (a) shows the operation of the tap control ($t_{5,j,sc}^{\text{VR}}$), where the effects of the saturation of VR control can be identified for the case when $t_{5,j,sc}^{\text{VR}} = 16$. Additionally, Fig. 13 (b) depicts the nonlinear solution (power flow) obtained using $V_m^{\text{set,VR}}$ determined using our MILP model. In this figure a greater dispersion can be recognized in the tap positions within the regulation zone, which results in an increase of 0.36% in C^{oper}. By contrast, when the tap positions given by our MILP model are used in the power flow study, the result tends to the optimal solution, as shown

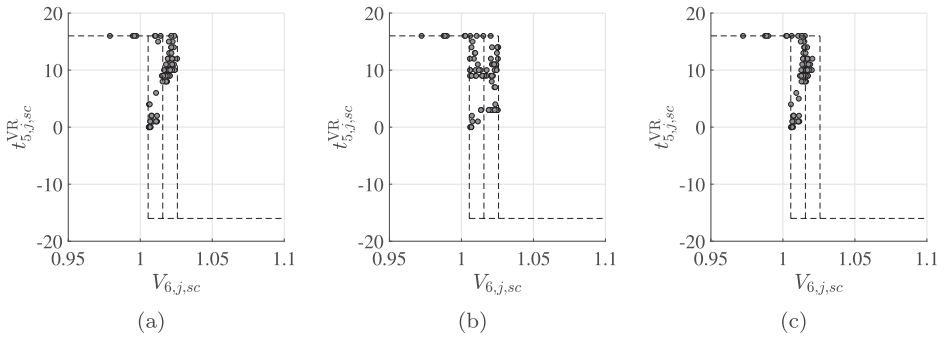

Fig. 13. Control of tap operation with a VR at node 5 of the 23-node system during VR Test, resulted from (a) proposed MILP, (b) power flow, and (c) power flow with defined taps.

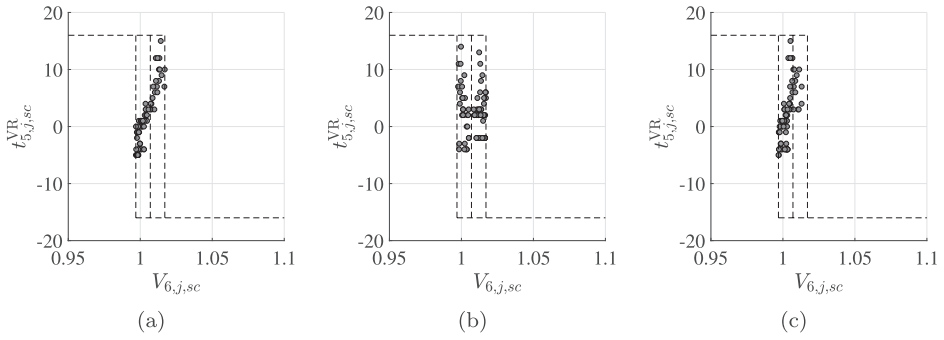

Fig. 14. Control of tap operation for a VR at node 5 of the 23-node system for CB + VR Test resulted from (a) proposed MILP, (b) power flow, and (c) power flow with defined taps.

Table 6
Summary of the MILP results for the 69-node system.

Test	C^{oper} [$\times 10^3$ US$]	Losses [MWh/year]	z [pu]	Processing time [s]
Base Case	108.10 (−2.90%)[a]	915.21 (0.56%)[b]	0.0847 (−0.0433)[c]	–
CB	77.32 (−1.50%)	672.36 (0.70%)	0.0384 (−0.0193)	81
VR	104.19 (−0.83%)	936.24 (0.39%)	0.0137 (−0.0146)	639
CB + VR	75.60 (−1.72%)	678.87 (0.05%)	0.0105 (−0.0156)	1223
Base Case DER	97.99 (−2.28%)	836.99 (0.79%)	0.0676 (−0.0344)	73
CB + DER	74.83 (−1.60%)	644.86 (1.00%)	0.0444 (−0.0219)	81
VR + DER	94.33 (−0.70%)	853.56 (0.38%)	0.0051 (−0.0117)	168
CB + VR + DER	66.30 (−1.25%)	599.73 (0.11%)	0.0037 (−0.0104)	915

[a] Percentual difference of operational costs in relation to power flow result.
[b] Percentual difference of power losses in relation to power flow result.
[c] Per unit difference of voltage violations in relation to power flow result.

in Fig. 13 (c).

The combination of CBs and VR results in the best solution since the energy losses decrease due to the presence of three CBs of 600 kvar, two fixed, and one automatic. Thus, the VR and CBs contribute to reducing the voltage violations, in comparison to the Base Case. Besides, no tap saturation could be observed for the VR, and the presence of fixed CBs resulted in negative taps, as shown in Fig. 14 (a). Note the difference between the results obtained with power flow studies using a VR control based on $V_m^{set,VR}$ (Fig. 14 (b)) and the results obtained with the taps determined with our MILP model (Fig. 14 (c)).

Table 7
Summary of the volt-var control results for the 69-node system.

Test	Capacitor Bank Node	Type	$I_m^{on,AI}$ [pu]	$I_m^{off,AI}$ [pu]	Voltage Regulator Node	$V_m^{set,VR}$ [pu]
Base Case	–	–	–	–	–	–
CB	50	A1200	0.1933	0.0849	–	–
VR	–	–	–	–	42	1.0275
CB + VR	50	A1200	0.1933	0.0849	42	1.0156
Base Case DER	–	–	–	–	–	–
CB + DER	50	A600	0.1931	0.0847	–	–
VR + DER	–	–	–	–	42	1.0275
CB + VR + DER	50	A600	0.1931	0.0847	42	1.0188

Regarding the tests containing DER, all VVC results listed in Table 5 are slightly larger when compared with the tests without DER. Moreover, using the proposed method, all results shown in Table 4 have been improved significantly in comparison with the Base Case; further, the CB + VR + DER Test shows that the best VVO solution was achieved for the 23-node system, as the lowest total cost resulted.

5.3. Results for the 69-node system

The results obtained from all tests with the 69-node system are shown in Table 6, and the VVC results are shown Table 7.

As can be seen in Table 6, for all cases analyzed, small divergences were observed between the results obtained with our MILP model and corresponding results obtained with power flow. Variations lower than 2.9% were detected in the operation costs, 1% in the energy losses, and 0.04 pu in voltage violations, thus proving the accuracy of the proposed model.

Similar to the results concerning the 23-node system, all results for

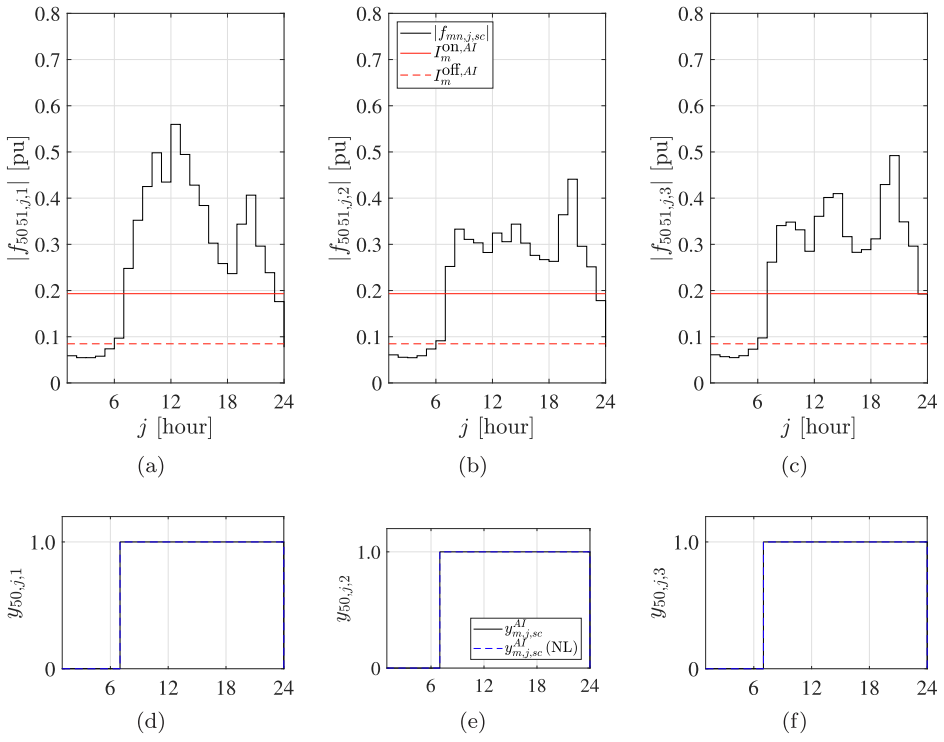

Fig. 15. Results obtained with a controlled CB at node 50 for the 69-node system from CB + VR + DER Test: (a)-(c) hourly monitored downstream branch current during scenarios 1, 2, and 3, respectively; (d)-(f) hourly CB state during scenarios 1, 2, and 3, respectively.

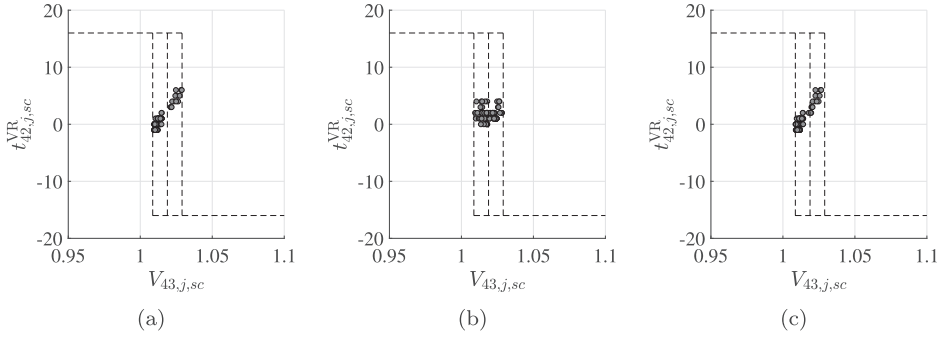

Fig. 16. Tap operation control with a VR at node 43 for the 69-node system for CB + VR + DER Test resulted from (a) proposed MILP, (b) power flow, and (c) power flow with defined taps.

DER with the 69-node system indicated an improvement in the operation costs, and the CB + VR + DER Test indicated a reduction of 38% in the operation costs in relation to the Base Case. The loaded node 50 has the biggest reactive demand of the feeder (888 kvar), so that a CB is required at this node working from 7 a.m. to midnight during the whole year, as illustrated in Fig. 15. Consequently, this test shows that a reduction of 237 MWh/year in energy losses is possible.

The presence of VRs reduce voltage violations, but increases the energy losses, when compared with the Base Case. However, the CB + VR combination decreases the energy losses and the voltage violations, as expected. We observed that this system has no voltage problems even in the Base Case, since the annual voltage violation (z) is nearly zero. As a consequence, voltage saturation did not appear in the control of the tap operation, as shown in Fig. 16 for CB + VR + DER Test.

As a final remark, the results for both systems and the short processing times required for all tests confirm the computational efficiency of the proposed MILP model.

5.3.1. *Comparison with a previous study*

We used the 69-node system to compare our MILP model with a previous MILP model proposed in [44] for PDS expansion planning. The model presented in [44] differs from our model in the following aspects: (i) only one duration curve is used to model the load behavior; (ii) the load is represented as constant real and reactive power; (iii) the formulation has no current variables to control the switching of CBs; (iv) the VR control is based on tap position, which is represented as a continuous variable, with no prescribed voltages to be held by a VR; (v) the adjustment of VR precludes the use of line drop compensators; (vi) the solution of VR control can become infeasible because it has no saturation; (vii) the MILP model offers no possibility to limit the operation of CBs and VRs. The main aspects that distinguish our model from [44] are listed in Table 8, where the second column shows the characteristics of the MILP proposed by [44] and the third the characteristics of our model.

Therefore, to better compare the characteristics of our model and those of the model proposed in [44], we applied our model to two tests using the 69-node system, as shown in columns 4 and 5 of Table 8 (Test 1

Table 8
Comparison of our approach with that in [44].

	Aspect	Ref. [44]	Proposed MILP model		
			Original formulation	Test 1 approach	Test 2 approach
i.	load profile	duration curve with three load levels	daily load curve and *sc* scenarios	duration curve with three load levels	duration curve with three load levels
ii.	load model	constant P	constant I	constant I	constant I
iii.	CB control	load level	current	load level	current
iv.	VR control	tap position	voltage set	tap position	voltage set
v.	Line drop compensator	no	yes	no	yes
vi.	VR operation with saturation	no	yes	no	yes
vii.	daily switching limits of VVC devices	no	yes	no	no

Table 9
Summary of the VVC results of Case CB + VR for the 69-node system.

VVC device		Ref. [44]	Proposed MILP	
			Test 1	Test 2
Capacitor Bank	Node	50	50	50
	Type	F900	F900	A900
	$I_m^{on,AI}$ [pu]	–	–	0.10
	$I_m^{off,AI}$ [pu]	–	–	0.00
	$y_{50,1,1}^{AI}$ [pu]	1	1	1
	$y_{50,2,1}^{AI}$ [pu]	1	1	1
	$y_{50,3,1}^{AI}$ [pu]	1	1	1
Voltage Regulator	Node	44	44	44
	Remote node of LDC	–	–	46
	$V_m^{set,VR}$ [pu]	–	–	0.9724
	$t_{44,1,1}^{VR}$	5	5	4
	$t_{44,2,1}^{VR}$	3	3	1
	$t_{44,3,1}^{VR}$	2	2	−3

Table 10
Results for Case CB + VR of the 69-bus system.

Results	Ref. [44]	Proposed MILP	
		Test 1	Test 2
C^{oper} [$\times 10^3$]	49.64	47.44	46.86
Losses [MWh/year]	827.38	789.68	781.09
z [pu]	0.00	0.00	0.00

and Test 2). For Test 1 we kept the same conditions of [44], except for the load representation, while for Test 2 we considered our VVC approach, but keeping the original load levels. Further, we fixed the substation voltage at 1.0 pu and limited the voltages of loaded nodes to the interval [0.95,1.0] pu. Three load levels were considered, 1.0 pu, 0.8 pu and 0.5 pu, with respective durations of 1000, 6760 and 1000 h/year. Besides, we used VRs with maximum current of 200 A, and switched CBs with nominal power of 900 kvar. Finally, we assumed 0.06 US$/kWh as energy costs.

Table 9 summarizes the results for VVC obtained with our MILP model for the 69-node system considering the case study CB + VR. On the other hand, Table 10 contains the solutions obtained by [44] for Tests 1 and 2 in terms of operation cost, energy losses, and voltage violations.

Concerning Test 1, we disregarded some features of the proposed method and considered the optimal solution of CB and VR allocation problem obtained by [44] to adjust the CB control and the tap positions of VRs. This test gave similar results for both linearized models. We also observed that the slightly lower losses obtained by our model are due to the characteristics of the load model adopted (constant current instead of constant power).

Since our approach uses explicit variables to determine both the current control of switched CBs and the voltage reference at the output of the VR, during Test 2 the MILP model searched the minimum operation cost and the minimum of VVC variables of CBs and VRs. Thus, regarding the CB control, the proposed MILP model defined the same operation point as defined by [44], where the original solution contains a fixed CB unit; in contrast, our solution has an uninterrupted operation of the switched CB. However, concerning VR control, the resulting tap positions are 4, 1, and −3, for loading levels 1 to 3, respectively. Note that these values, although slightly different from those obtained by [44], allowed to reduce operating costs in comparison to the results of Test 1.

5.4. Application of the proposed model to a large system

To further check the validity and flexibility of the proposed method, it was applied to an existing distribution feeder located in the south of Brazil. This feeder has 733 buses (see Fig. 17), operates at 13.8 kV, and has a total line length of 17.5 km. Besides, this system has 185 mm^2 XLPE, 336.4 MCM, and 1/0 AWG aluminum conductors and feeds 188 load buses in an urban area; the voltage magnitude at the substation bus was assumed as 1 pu. Based on a previous planning study presented in [8], we considered also a DER unit with 1.5 MW of nominal power, installed at node 278, as well as two automatic CBs, with a unit of 600 kvar installed at node 202 and another unit of 1200 kvar at node 349.

To model the chronological operation of all 188 loaded nodes, we considered three typical load profiles, all of them used by the utility, to represent a business day, Saturday, and Sunday, as depicted in Fig. 18.

The results obtained from all tests with the 733-node system are shown in Table 11, and the VVC results are shown Table 12. According to Table 11, a comparison of the total operational cost of the Case CB with the cost of Base Case reveals a reduction of 48.7%, which can be explained by the reduction in the energy losses and voltage violations. However, the lowest operation cost resulted for the Case CB + DER, for which we observed a reduction of 72% compared to the Base Case. These results demonstrated the importance of including possible contribution of DERs to achieve better solutions regarding the minimization of energy losses and voltage profile improvement. The operation point of the DER is illustrated in Fig. 19, from which we recognize that the model determines the active and reactive current injection so as to minimize the total costs.

The results of the real distribution system with 733 nodes thus far analyzed demonstrate the flexibility of the proposed model. It can also be concluded that the number of volt-var devices to be controlled has a greater impact on the solutions obtained compared with the impact of the number of nodes/buses. Further, since the solution search space of volt-var optimization problems is proportional to the number of operation modes of loads and DERs, it becomes essential to find the optimal solution with high accuracy and within reasonable processing time. It is also worth mentioning that the concept of what can be considered as a suitable model changes over time, as very complex models may become suitable only in the future when new solution techniques and/or more powerful computers become available.

Although the proposed method proved to have many advantages, it also has some limitations and drawbacks: (i) concerning CBs, although the MILP includes current hysteresis control, the simultaneous control of current and voltage is not available in this model; (ii) in relation to VRs, the proposed voltage control does not consider the direction of the

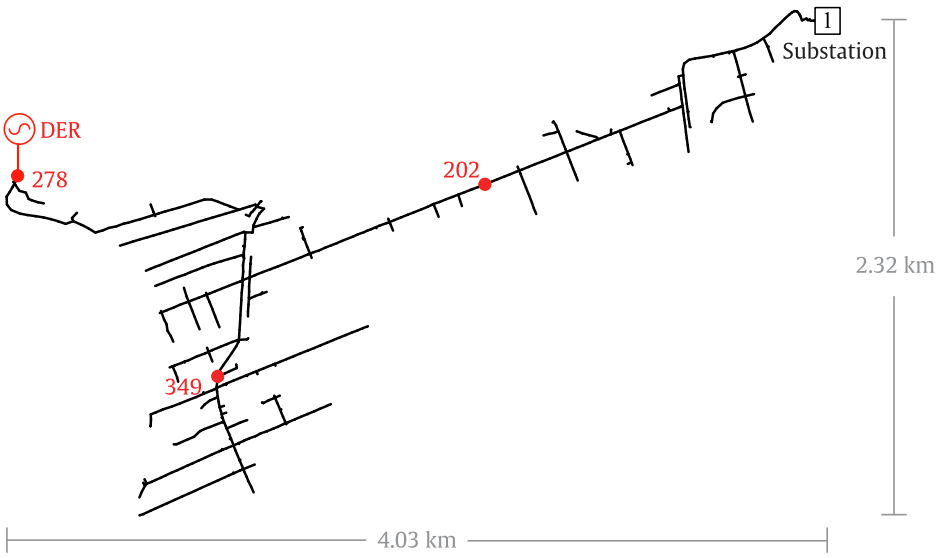

Fig. 17. Diagram of the 733-node system [8].

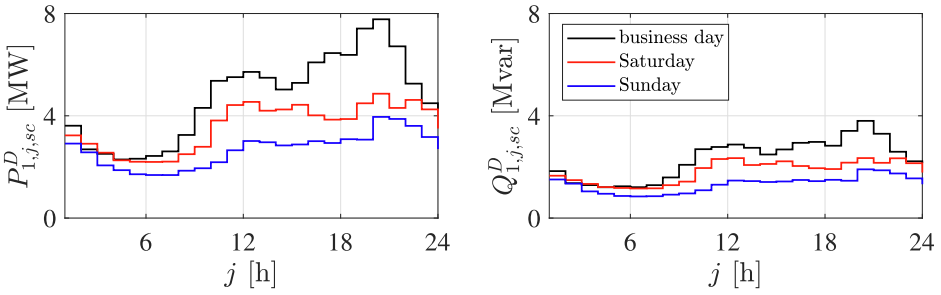

Fig. 18. Aggregated profiles of hourly active and reactive power demands at substation of the 733-node system during a typical business day, Saturday, and Sunday.

Table 11
Summary of the results for the proposed MILP applied to the 733-node system.

Test	C^{oper} [$\times 10^3$ US$]	Losses [MWh/year]	z [pu]	Processing time[4] [s]
Base Case	100.82 (0.24%)[1]	504.00 (0.46%)[2]	0.5181 (–0.0001)[3]	900
CB	51.69 (0.16%)	422.31 (0.54%)	0.0598 (–0.0018)	975
CB + DER	28.26 (1.24%)	255.95 (1.18%)	0.0012 (0.0002)	2080

[1] Percentage difference of operational costs in relation to power flow result.
[2] Percentage difference of power losses in relation to power flow result.
[3] Per unit difference of voltage violations in relation to power flow result.
[4] For this system, the optimality gap (relative MIP gap tolerance [39]) was chosen as 10^{-2}.

Table 12
Summary of the results for the 733-node system in the case of volt-var control.

Test	DER Node	Mode	Capacitor Bank Node	Type	$I_m^{on,AI}$ [pu]	$I_m^{off,AI}$ [pu]
Base Case	–	–	–	–	–	–
CB	–	–	202	A600	0.1500	0.0000
	–	–	349	A1200	0.8579	0.6435
CB + DER	278	PF range	202	A600	1.2171	1.0155
			349	A1200	0.8952	0.7229

current flow; such a feature would demand the inclusion of new disjunctive constraints; (iii) the contribution of DER to VVO problem has not been widely considered, thus the power capability (Q-capability) of DER needs to be further explored, as proposed by [17]; (iv) the use of K-means clustering to model the chronological operation in fact reduces the amount of data; however, the use of centroids to represent the cluster can increase the error, since outliers can dominate the computation of the average.

6. Conclusions

This paper proposed a MILP model for VVO which considers the chronological operation of PDS containing DERs. Essentially, the model supports operation planning decisions in PDS and can optimally adjust VVC devices based on the steady-state operation of each time interval contained in typical daily scenarios.

In contrast to previous methods found in the literature, the proposed approach consists of a novel formulation for the current control of automatic CBs and tap operation control of VRs with LDC. One of the outstanding advantages of the proposed model is a decentralized approach in which the VVC devices are locally controlled, ensuring the converge to optimal solution of feeders, thus closely resembling the utility reality. Besides, the MILP model allows solving the problem through exact optimization techniques. Concerning the VVO strategy, the model considers (i) current hysteresis control of CBs, thus making them sensitive to downstream load variations; (ii) the saturation of the VR control, allowing them to operate taps and help find optimal solutions; (iii) the possibility to analyze VRs with line drop compensation. Furthermore, the model allows selecting scenarios to model the chronological operation and to preserve the inherent simultaneity of

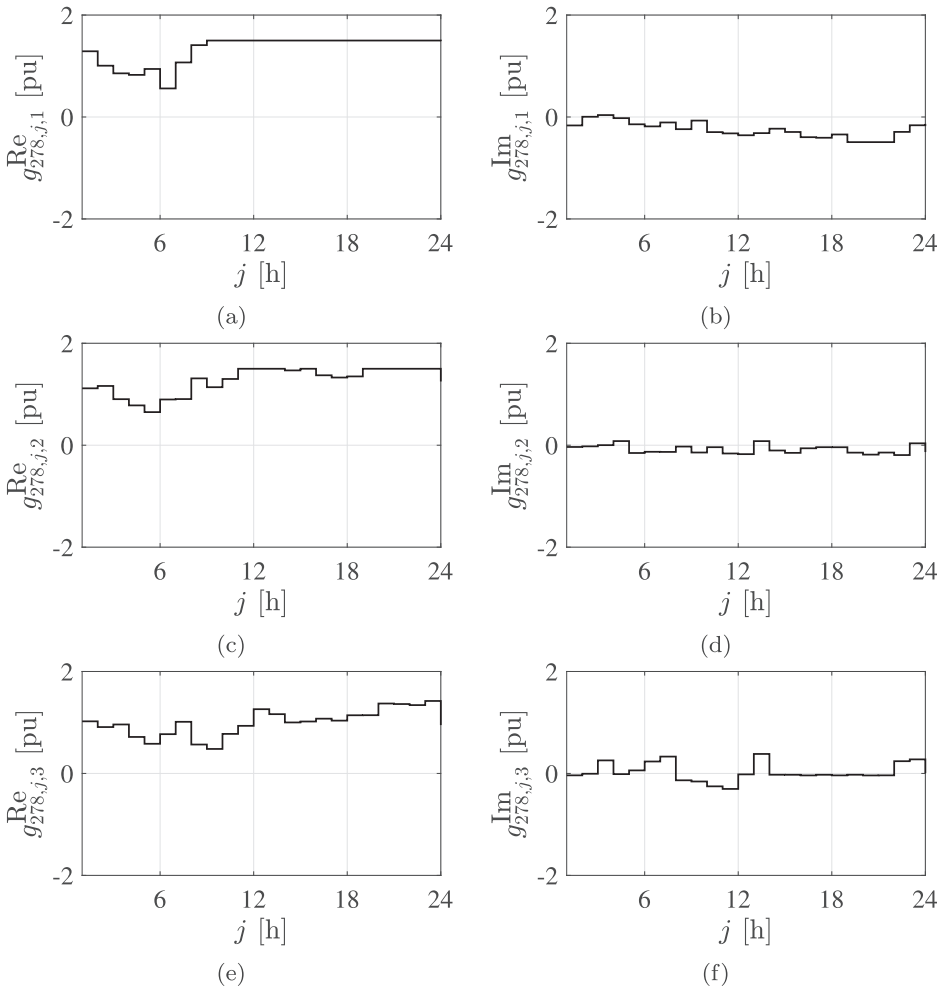

Fig. 19. Hourly active and reactive power profiles of DER operating at node 278 of the 733-node system during a typical: (a)–(b) business day; (c)–(d) Saturday; and (e)–(f) Sunday.

multiple loads and DERs.

To illustrate the potential of the proposed model, the optimal operation of CBs and VRs were obtained independently, and also integrated into the same test. The results of tests with systems containing 23, 69, and 733 nodes indicate a very good agreement with corresponding results obtained through power flow studies, even with an expressive variation of load levels and the number of DERs. Further, the efficiency and robustness of the proposed MILP model have been demonstrated by the low processing time of all tests.

In summary, our solution approach has the following characteristics:

1. we define more realistic operation scenarios by considering relevant factors, such as the sensitivity of VVC devices to variations in load demands and DER power injections;
2. we model the chronological operation so as to reduce the redundancy of information taking into account relevant characteristics of each load and DER;
3. we take the temporal sequencing into account to limit the number of daily on/off switchings of automatic CBs and tap operation of VRs, thus avoiding an excessive number of switchings which may cause transients, increase maintenance costs, and reduce the life of VVC devices.

Due to the growing number of advanced metering infrastructures of smart grids, an expressive amount of load data is nowadays available. Therefore, further development of the model presented in this paper includes a formulation to deal with high-level uncertainties related to the behavior of loads and DERs.

CRediT authorship contribution statement

Bibiana P. Ferraz: Conceptualization, Methodology, Software, Validation, Formal analysis, Investigation, Resources, Writing - original draft, Writing - review & editing. **Mariana Resener:** Conceptualization, Methodology, Software, Resources, Writing - review & editing. **Luís A. Pereira:** Writing - review & editing, Visualization. **Flávio A.B. Lemos:** Validation, Visualization. **Sérgio Haffner:** Conceptualization, Methodology, Writing - review & editing, Supervision, Funding acquisition, Project administration.

Declaration of Competing Interest

The authors declare that they have no known competing financial interests or personal relationships that could have appeared to influence the work reported in this paper.

Acknowledgments

This study was financed in part by the Coordenação de Aperfeiçoamento de Pessoal de Nível Superior - Brasil (CAPES) - Finance Code 001. The authors also thank the brazilian funding agency CNPq for the grant number 306126/2019-2.

Appendix A. PWL approximation of $\left|f_{mn,j,sc}\right|$

Similar to univariate functions, bivariate functions can be linearized by plans instead line segments [45]. Hence, we propose a convex combination model using PWL functions to approximate bivariate mixed-integer function. Based on [7], this approach makes possible to use binary variables to select each plan that approximates the nonlinear function, and thus calculate the current magnitude as a convex combination of vertices. Formally, the model is expressed as follows, with $\forall\rho = \{1,\ldots,n_\rho\}$ and n_ρ as the number of adopted plans.

$$c^{\mathrm{Re}}(v) = f^{\max}\cos\left[\frac{2\pi}{n_\rho}(i-1)\right], \tag{A.1}$$

$$c^{\mathrm{Im}}(v) = f^{\max}\sin\left[\frac{2\pi}{n_\rho}(i-1)\right], \tag{A.2}$$

$$c^{f}(v) = f^{\max}, \tag{A.3}$$

$$\sum_{\rho\in\mathscr{P}}\sum_{v\in\mathscr{V}(\rho)} \alpha^{\rho v}_{mn,j,sc}\, c^{\mathrm{Re}}(v) = f^{\mathrm{Re}}_{mn,j,sc}, \tag{A.4}$$

$$\sum_{\rho\in\mathscr{P}}\sum_{v\in\mathscr{V}(\rho)} \alpha^{\rho v}_{mn,j,sc}\, c^{\mathrm{Im}}(v) = f^{\mathrm{Im}}_{mn,j,sc}, \tag{A.5}$$

$$\sum_{\rho\in\mathscr{P}}\sum_{v\in\mathscr{V}(\rho)} \alpha^{\rho v}_{mn,j,sc}\, c^{f}(v) = \left|f_{mn,j,sc}\right|, \tag{A.6}$$

$$\alpha^{\rho v}_{mn,j,sc} \geqslant 0,\ \ \forall\rho\in\mathscr{P} = \{\rho_1,\ldots,\rho_{n_\rho}\},\ \ \forall v\in\mathscr{V}(\rho) = \{v_0, v_\rho, v_{\rho+1}\}, \tag{A.7}$$

$$\sum_{v\in\mathscr{V}(\rho)} \alpha^{\rho v}_{mn,j,sc} = s^{\rho}_{mn,j,sc},\ \ \forall\rho\in\mathscr{P}, \tag{A.8}$$

$$\sum_{\rho\in\mathscr{P}} s^{\rho}_{mn,j,sc} = 1. \tag{A.9}$$

The model thus defined is detailed through the example in Fig. A.1, where the current magnitude is represented by a two dimensional PWL with 12 plans, and where each plan is represented by 3 vertices. Then, $c^{\mathrm{Re}}(v)$, $c^{\mathrm{Im}}(v)$, and $c^{f}(v)$are the vertices of each plan used for PWL and $f^{\max}$ is the maximum value that each variable could assume under linearization. In this way, expressions (A.8) and (A.9) represent constraints that enable just one plan ρ for each time step j and scenario sc through the binary variables $s^{\rho}_{mn,j,sc}\in\{0,1\},\ \forall\rho\in\mathscr{P}$. Considering that the plan ρ_1 is enabled $\left(s^{\rho_1}_{mn,j,sc}=1\right)$, then $\alpha^{\rho_1 v}_{mn,j,sc}$ assumes values inside the interval $[0,1]$, in order to parameterize the convex combinations of vertices. Note that $\alpha^{\rho v}_{mn,j,sc}$ of the remaining plans (ρ_2 to ρ_{12}) are canceled, since $s^{\rho}_{mn,j,sc}=0,\ \forall\rho=\{2,..,12\}$. The constraints (A.4)–(A.7) represent the weights for all vertices, previously calculated through expressions (A.1)-(A.3) considering the enabled plan ρ_1. Finally, the balance between computational burden and the error of the convex combination model of PWL provides information for decision-making on the best number of plans.

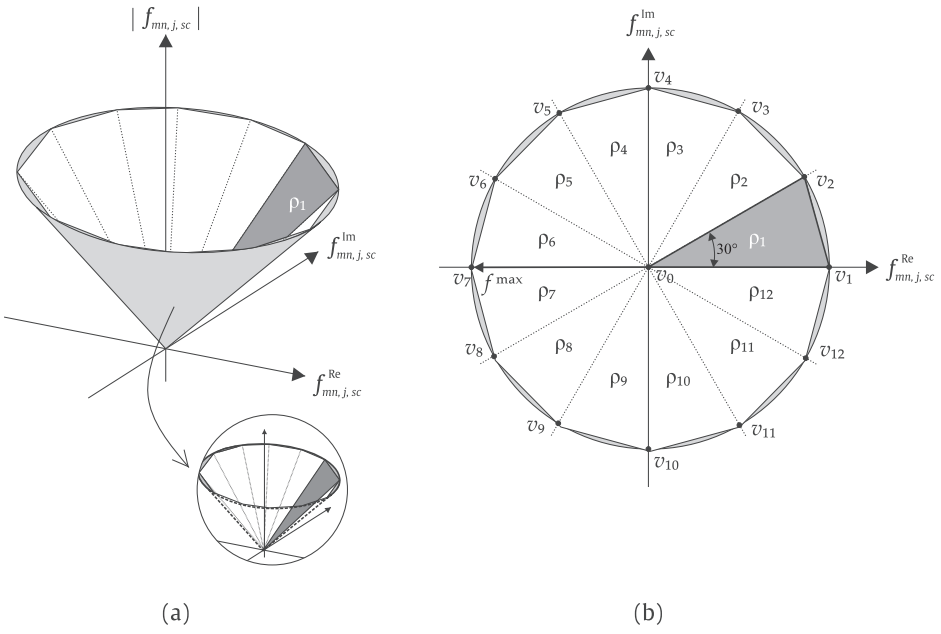

Fig. A.1. Example of the proposed PWL to approximate a bivariate function: (a) 3D-view of convex combination model; (b) 2D-view of adopted plans.

The procedure described can be used to limit the convex combination to only one plan during the time step j and scenario sc. Moreover, $f^{\mathrm{Re}}_{mn,j,sc}$ and $f^{\mathrm{Im}}_{mn,j,sc}$ are independent variables of the non-convex function to be linearized, and the term $\left|f_{mn,j,sc}\right|$ is assumed to be the magnitude of the downstream branch current, which is further used in the current control of automatic CBs (see Section 3.2.2).

Appendix B. Voltage violations

Regulators can impose financial penalties on distribution utilities for not complying with the prescribed limits of node voltages. Therefore, the allowable voltage limits are also considered in the proposed model and expressed as follows [8].

$$z_{m,j,sc} = \begin{cases} V_{m,j,sc} - V_m^{\max}, & \text{if } V_{m,j,sc} > V_m^{\max} \\ V_m^{\min} - V_{m,j,sc}, & \text{if } V_{m,j,sc} < V_m^{\min} \\ 0, & \text{otherwise.} \end{cases} \tag{B.1}$$

Above, $z_{m,j,sc}$ stands for the voltage violation related to node m at the time step j and scenario sc; $V_{m,j,sc}$ represents the voltage magnitude, while and $V_m^{\max}$ and $V_m^{\min}$ represent the voltage limits. On the other hand, the annual voltage violation is determined from the expression below.

$$z = \sum_{sc\in\psi^K} \Delta T_{sc} \sum_{j\in\psi^J} \sum_{m\in\psi^D} z_{m,j,sc}. \tag{B.2}$$

To reduce the number of variables to be handled, the voltage limits as given by (B.1) can be stated by means of an optimization problem, which is defined as below.

$$\begin{aligned} \min \quad & z_{m,j,sc} \\ \text{s.t.} \quad & z_{m,j,sc} \geq V_{m,j,sc} - V_m^{\max}, \\ & z_{m,j,sc} \geq V_m^{\min} - V_{m,j,sc}, \\ & z_{m,j,sc} \geq 0. \end{aligned} \tag{B.3}$$

The mathematical expressions of voltage violation limits thus far described are illustrated in Fig. B.2.

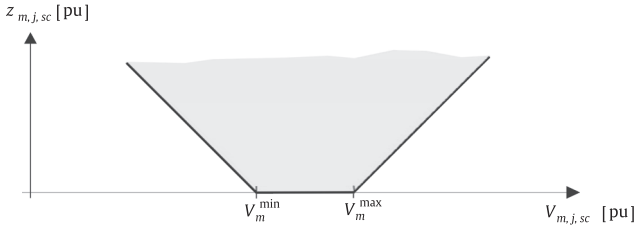

Fig. B.2. Representation of the expressions for voltage violations.

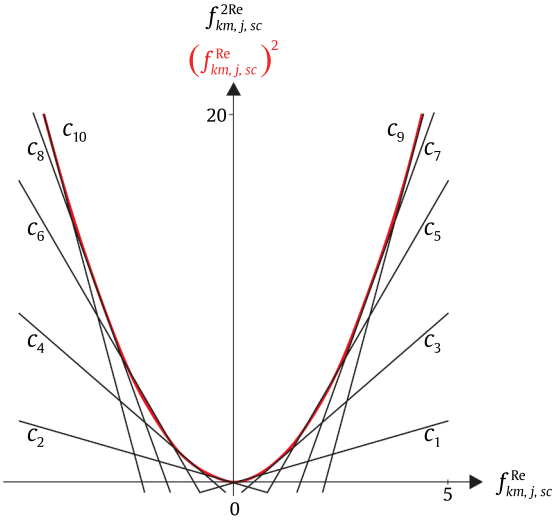

Fig. C.3. Example of a PWL representation of $\left(f^{\mathrm{Re}}_{km,j,sc}\right)^2$ using 10 linear constraints [33].

Appendix C. Power losses

In the proposed model, we estimate the power losses employing a univariate function, so that the current flowing in each branch is determined through PWL functions. Firstly, the current ($f_{km,j,sc}$) in each branch km can be positive as well as negative and expressed as:

$$f_{km,j,sc} = f^{\mathrm{Re}}_{km,j,sc} + f^{\mathrm{Im}}_{km,j,sc}. \tag{C.1}$$

Secondly, the power losses associated with branch km during the time step j and scenario sc are expressed by:

$$P^{\mathrm{loss}}_{km,j,sc} = R_{km}\left|\left(f^{\mathrm{Re}}_{km,j,sc}\right)^2 + \left(f^{\mathrm{Im}}_{km,j,sc}\right)^2\right|, \tag{C.2}$$

where R_{km} stands for the real part of the impedance of branch km. Besides, we approximate the non-linear terms $f^{2\mathrm{Re}}_{km,j,sc}$ and $f^{2,\mathrm{Im}}_{km,j,sc}$ using linear expressions [33] (see Fig. C.3), from which there results:

$$\left(f^{\mathrm{Re}}_{km,j,sc}\right)^2 \approx f^{2\mathrm{Re}}_{km,j,sc} \geqslant a_h f^{\mathrm{Re}}_{km,j,sc} + b_h, \tag{C.3}$$

$$\left(f^{\mathrm{Im}}_{km,j,sc}\right)^2 \approx f^{2\mathrm{Im}}_{km,j,sc} \geqslant a_h f^{\mathrm{Re}}_{km,j,sc} + b_h, \tag{C.4}$$

Above, $h = 1, 2, \ldots, N^{LC}$ and b_h are constants, whereas N^{LC} represents the number of linear constraints. With the given approximations, the power losses can now be expressed as:

$$P^{\mathrm{loss}}_{km,j,sc} \approx R_{km} f^{2,\mathrm{Re}}_{km,j,sc} + R_{km} f^{2,\mathrm{Im}}_{km,j,sc}. \tag{C.5}$$

Finally, note that the accuracy of the approximation depends on the number of linear constraints used; further, including the terms $f^{2,\mathrm{Re}}_{km,j,sc}$ and $f^{2,\mathrm{Im}}_{km,j,sc}$ into the objective function makes the approximation valid, given that these terms are also minimized when the solution of the optimization problem is found.

Appendix D. Supplementary material

Supplementary data associated with this article can be found, in the online version, at https://doi.org/10.1016/j.ijepes.2021.106761.

References

[1] Resener M, Haffner S, Pereira LA, Pardalos PM. Optimization techniques applied to planning of electric power distribution systems: a bibliographic survey. Energy Syst 2018;9(3):473–509.

[2] Vítor TS, Asada EN, Vieira JCdM. Optimal volt/var control applied to modern distribution systems. In: Resener M, Rebennack S, Haffner PS, editors. Handbook of optimization in electric power distribution systems. Springer; 2020. p. 1–56.

[3] Jha RR, Dubey A, Liu C-C, Schneider KP. Bi-level volt-var optimization to coordinate smart inverters with voltage control devices. IEEE Trans Power Syst 2019;34(3):1801–13.

[4] Pamshetti VB, Singh S, Singh SP. Combined impact of network reconfiguration and volt-var control devices on energy savings in the presence of distributed generation. IEEE Syst J 2019:1–12.

[5] Ceylan O, Liu G, Tomsovic K. Coordinated distribution network control of tap changer transformers, capacitors and pv inverters. Electr Eng 2018;100(2):1133–46.

[6] Yilmaz M, El-Shatshat R. State-based volt/var control strategies for active distribution networks. Int J Electr Power Energy Syst 2018;100:411–21.

[7] Camponogara E, de Almeida KC, Junior RH. Piecewise-linear approximations for a non-linear transmission expansion planning problem. IET Gener Transm Distrib 2015;9(12):1235–44.

[8] Resener M, Haffner S, Pereira LA, Pardalos PM. Mixed-integer LP model for volt/var control and energy losses minimization in distribution systems. Electr Power Syst Res 2016;140:895–905.

[9] Resener M, Haffner S, Pereira LA, Pardalos PM, Ramos MJ. A comprehensive MILP model for the expansion planning of power distribution systems–part i: Problem formulation. Electr Power Syst Res 2019;170:378–84.

[10] Resener M, Haffner S, Pereira LA, Pardalos PM, Ramos MJ. A comprehensive MILP model for the expansion planning of power distribution systems–part ii: Numerical results. Electr Power Syst Res 2019;170:317–25.

[11] Ahmadi H, Martí JR, Dommel HW. A framework for volt-var optimization in distribution systems. IEEE Trans Smart Grid 2014;6(3):1473–83.

[12] Macedo LH, Franco JF, Rider MJ, Romero R. Optimal operation of distribution networks considering energy storage devices. IEEE Trans Smart grid 2015;6(6):2825–36.

[13] Sabillon-Antunez C, Melgar-Dominguez OD, Franco JF, Lavorato M, Rider MJ. Volt-var control and energy storage device operation to improve the electric vehicle charging coordination in unbalanced distribution networks. IEEE Trans Sustain Energy 2017;8(4):1560–70.

[14] Borghetti A, Napolitano F, Nucci CA. Volt/var optimization of unbalanced distribution feeders via mixed integer linear programming. Int J Electr Power Energy Syst 2015;72:40–7.

[15] Ramadhani UH, Shepero M, Munkhammar J, Widén J, Etherden N. Review of probabilistic load flow approaches for power distribution systems with photovoltaic generation and electric vehicle charging. Int J Electr Power Energy Syst 2020;120:106003.

[16] Samimi A, Kazemi A. Scenario-based stochastic programming for volt/var control in distribution systems with renewable energy sources. IETE Tech Rev 2016;33(6):638–50.

[17] Samimi A, Kazemi A, Siano P. Economic-environmental active and reactive power scheduling of modern distribution systems in presence of wind generations: A distribution market-based approach. Energy Convers Manage 2015;106:495–509.

[18] Samimi A, Kazemi A. Coordinated volt/var control in distribution systems with distributed generations based on joint active and reactive powers dispatch. Appl Sci 2016;6(1):4.

[19] Samimi A, Nikzad M, Siano P. Scenario-based stochastic framework for coupled active and reactive power market in smart distribution systems with demand response programs. Renew Energy 2017;109:22–40.

[20] Samimi A, Nikzad M. Complete active-reactive power resource scheduling of smart distribution system with high penetration of distributed energy resources. J Modern Power Syst Clean Energy 2017;5(6):863–75.

[21] Samimi A, Kazemi A. A new market-based approach for daily volt/var control of distribution systems in the presence of distributed energy resources using benders decomposition algorithm. Turkish J Electr Eng Comput Sci 2016;24(5):3741–58.

[22] Teichgraeber H, Brandt AR. Clustering methods to find representative periods for the optimization of energy systems: An initial framework and comparison. Appl Energy 2019;239:1283–93.

[23] Zatti M, Gabba M, Freschini M, Rossi M, Gambarotta A, Morini M, Martelli E. k-milp: A novel clustering approach to select typical and extreme days for multi-energy systems design optimization. Energy 2019;181:1051–63.

[24] Jain AK. Data clustering: 50 years beyond K-means. Pattern Recogn Lett 2010;31(8):651–66.

[25] Moradijoz M, Moghaddam MP, Haghifam M. A flexible active distribution system expansion planning model: a risk-based approach. Energy 2018;145:442–57.

[26] Li R, Wang W, Xia M. Cooperative planning of active distribution system with renewable energy sources and energy storage systems. IEEE Access 2018;6:5916–26.

[27] Sannigrahi S, Roy Ghatak S, Acharjee P. Multi-scenario based bi-level coordinated planning of active distribution system under uncertain environment. IEEE Trans Ind Appl 2019:1–12.

[28] Li R, Wang W, Chen Z, Jiang J, Zhang W. A review of optimal planning active distribution system: models, methods, and future researches. Energies 2017;10 (11):1715.
[29] Hagh MT, Amiyan P, Galvani S, Valizadeh N. Probabilistic load flow using particle swarm optimization clustering method. IET Gener Transmiss Distrib 2018;12(3): 780–9.
[30] Home-Ortiz JM, Pourakbari-Kasmaei M, Lehtonen M, Mantovani JRS. Optimal location-allocation of storage devices and renewable-based DG in distribution systems. Electr Power Syst Res 2019;172:11–21.
[31] Ferraz BP, Júnior JDA, Lemos F, Haffner S. Analysis of distribution system considering load uncertainties: a K-means clustering approach. In: IEEE PES Innovative Smart Grid Technologies Conference-Latin America (ISGT Latin America). IEEE; 2019. p. 1–6.
[32] Tibshirani R, Walther G, Hastie T. Estimating the number of clusters in a data set via the gap statistic. J Roy Stat Soc Ser B (Stat Methodol) 2001;63(2):411–23.
[33] Resener M, Haffner S, Pardalos PM, Pereira LA. A convex model for the optimization of distribution systems with distributed generation. In: BertschWolf V, Fichtner W, Heuveline V, Leibfried T, editors. Advances in energy system optimization. Springer; 2017. p. 231–45.
[34] Kersting WH. Distribution system modeling and analysis. CRC Press; 2012.
[35] Pflugradt N. Load profile generator (version 1.3.5); 2018. https://www.loadprofilegenerator.de.
[36] Pfenninger S, Staffell I. Long-term patterns of european pv output using 30 years of validated hourly reanalysis and satellite data. Energy 2016;114:1251–65.
[37] Staffell I, Pfenninger S. Using bias-corrected reanalysis to simulate current and future wind power output. Energy 2016;114:1224–39.
[38] Van Hentenryck P. The OPL optimization programming language. MIT; 1999.
[39] IBM. Software CPLEX Optimization Studio v 12.9.0.0; 2019.
[40] Dugan RC. Software OpenDSS (version 7.6.5.52). Electric Power Research Institute (EPRI); 2018. URL http://smartgrid.epri.com/SimulationTool.aspx.
[41] MathWorks. Software matlab (version r2019a); 2019. http://mathworks.com.
[42] Haffner S, Pereira LFA, Pereira LA, Barreto LS. Multistage model for distribution expansion planning with distributed generation–Part II: Numerical results. IEEE Trans Power Deliv 2008;23(2):924–9.
[43] Baran ME, Wu FF. Optimal capacitor placement on radial distribution systems. IEEE Trans Power Deliv 1989;4(1):725–34.
[44] Franco JF, Rider MJ, Lavorato M, Romero R. A mixed-integer lp model for the optimal allocation of voltage regulators and capacitors in radial distribution systems. Int J Electr Power Energy Syst 2013;48:123–30.
[45] Keller M, Karl H. Response-time-optimised service deployment: MILP formulations of piece-wise linear functions approximating non-linear bivariate mixed-integer functions. IEEE Trans Netw Serv Manage 2017;14(1):121–35.